NATIONAL AERONAUTICS AND SPACE ADMINISTRATION

Technical Report 32-1605

Conical-Scan Tracking With the 64-m-diameter Antenna at Goldstone

JET PROPULSION LABORATORY
CALIFORNIA INSTITUTE OF TECHNOLOGY
PASADENA, CALIFORNIA

October 1, 1976

NATIONAL AERONAUTICS AND SPACE ADMINISTRATION

Technical Report 32-1605

Conical-Scan Tracking With the 64-m-diameter Antenna at Goldstone

J. E. Ohlson
Naval Postgraduate School

M. S. Reid
Jet Propulsion Laboratory

JET PROPULSION LABORATORY
CALIFORNIA INSTITUTE OF TECHNOLOGY
PASADENA, CALIFORNIA

October 1, 1976

Preface

The work described in this report was performed by the Telecommunications Division of the Jet Propulsion Laboratory. Dr. John E. Ohlson is Associate Professor of Electrical Engineering at the Naval Postgraduate School and a consultant to the Laboratory.

Acknowledgment

The authors acknowledge considerable help from, and many useful discussions with, D. Girdner of DSS-14 in the experimental implementation of conical-scan tracking on the 64-m-diameter antenna reported upon in Section VI of this report.

Contents

Tables

Figures

Abstract

This report documents the theory and experimental work which demonstrated the feasibility of conical-scan tracking with the NASA/Jet Propulsion Laboratory 64-m-diameter paraboloid antenna at Goldstone, California. The purpose of this scheme is to actively track spacecraft and radio sources continuously with an accuracy superior to that obtained by manual correction of the computer-driven pointing. The conical-scan implementation gives increased tracking accuracy with X-band spacecraft signals, as demonstrated in the Mariner Venus/Mercury 1973 mission. Also, the high accuracy and ease of measurement with conical-scan tracking allow evaluation of systematic and random antenna tracking errors.

Conical-Scan Tracking With the 64-m-diameter Antenna at Goldstone

I. Introduction

The 64-m-diameter NASA/JPL paraboloid antenna at Goldstone, California, is used for communication with many spacecraft. It is also used for research in such supporting areas as planetary radar, interferometry, and radiometry. For conventional pointing, the antenna employs a "master equatorial" mechanical reference which is located at the intersection of the azimuth and elevation axes. The master equatorial is driven by a computer, and the antenna is slaved to the master equatorial by a large servo system which constitutes the azimuth and elevation drive mechanisms. Although high off the ground, the master equatorial is atop its own separate structural tower and foundation and is protected from the wind and sun by appropriate shielding.

For S-band frequencies in the range of 2100 to 2400 MHz, the antenna has excellent pointing performance. The absolute pointing error is a small fraction of the antenna beamwidth at S-band, and for use there the antenna "tracks" a spacecraft or radio source by simply pointing in a computer-calculated direction. Active tracking schemes using monopulse or conventional conical-scan tracking were not installed on the antenna due to its excellent absolute pointing ability.

The Mariner Venus/Mercury 1973 mission, the first mission on which conical-scan tracking was used to track a spacecraft, had an X-band downlink as well as the usual uplink and downlink at S-band. With approximately a factor of 4 increase in frequency over S-band, the antenna beamwidth was reduced by the same factor. In mission planning, concern arose over the ability to keep the X-band antenna beam (approximately 0.038 deg wide at the half-power points) properly pointed so a gain loss would not occur. Implementation of a monopulse or conventional conical-scan tracking feed would somewhat degrade the system operating temperature and would entail substantial hardware modifications. Implementation of a conical-scan tracking scheme for radio sources by rotating an entire 26-m-diameter paraboloid antenna about tracking boresight had been done previously (Ref. 1). The idea was felt to be sound for spacecraft as well, and it was decided to implement it on the 64-m-diameter antenna. Also, a full analysis of the scheme was to be carried out. This report documents the results of this effort.

We will treat angle tracking of a noncoherent radio source first in Section III and then, in Section IV, consider tracking of a coherent source (spacecraft). The approach here assumes a basic knowledge of conical-scan tracking such as presented by Skolnik (Ref. 2). In Sections

III and IV, system gain fluctuations are ignored. This effect can dominate the system performance if the conical-scan rate is slower than the gain fluctuations. The reader should be aware that this will probably be the case for lobing done by moving the entire antenna. Then the results in Sections III and IV are optimistic and do not give the complete picture. If a faster scanning technique is employed in the future (e.g., feed or subreflector nutation) we might be able to ignore the gain fluctuations, and then Sections III and IV will give the complete system performance. In Section V, the effects of gain fluctuations will be considered in detail and the performance for arbitrary scan rates will be obtained. To summarize:

(1) Sections III and IV give tracking performance under the assumption that the scan rate is much faster than gain fluctuations.

(2) When lobing the entire antenna, this assumption is probably unjustified, but it might be justified if the scan rate were significantly increased in the future.

(3) Gain fluctuation effects are considered in Section V.

The remainder of this report covers the mechanics of implementation on the 64-m-diameter antenna (DSS-14) and the experimental results obtained thereby.

II. Preliminaries

The conical-scan scheme we shall employ here is essentially that which was proposed by G. Levy (Ref. 3) and successfully demonstrated with radio sources by R. Gosline on the NASA/JPL 26-m-diameter paraboloid DSS-13 at Goldstone, California (Ref. 1). This method had not been used with spacecraft until the present investigation.

Angle tracking is accomplished by lobing the antenna around boresight in a circular pattern with constant angular offset, called the scan radius or "squint" angle (see Fig. 1). "Boresight" refers to the entire system and not to the peak of the antenna gain pattern. Pointing "predicts" are used to direct boresight very close to the target and then the conical-scan lobing around boresight generates "offsets" to correct boresight for pointing errors. Generation of these offsets will be discussed shortly.

We henceforth assume the antenna beam to be circularly symmetric because asymmetry of the beam causes only second-order effects. If a spacecraft or radio source is on boresight, the received signal power in the antenna is constant with time. However, if the source is off boresight, a small sinusoidal variation in received power occurs. The frequency of the sinusoid is simply the conical-scan rate,

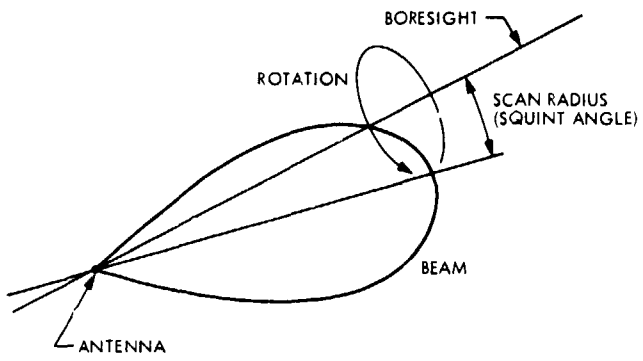

Fig. 1. Antenna geometry

the sinusoid amplitude is proportional to angular deviation of boresight from the source, and the phase of the sinusoid with respect to the conical-scan rotation gives the direction of the error.

Conical-scan schemes for radar tracking use sinusoid and cosinusoid signals referenced to the antenna lobing to do a correlation on the received signal strength to derive error signals for two orthogonal coordinates of the antenna, say elevation and cross-elevation (i.e., azimuth with secant correction). Radar tracking conventionally uses a relatively high scan rate of many cycles per second, so analog correlation suffices. However, for scan periods of 10-100 seconds the double-frequency terms arising in analog correlation would cause unwanted oscillation in the tracking system. Therefore, a scheme using integration over exactly one scan period and subsequent offset generation was chosen. This scheme is also compatible with current pointing offset procedures in the NASA/JPL Deep Space Network (DSN). The system block diagram is given in Fig. 2. The signal strength in Fig. 2 is taken as the output of a suitable radiometer when tracking a radio source. Careful attention must be paid to the time constant of the radiometer as we shall see later. The signal strength will be the receiver automatic gain control (AGC) voltage when tracking a spacecraft with coherent downlink carrier.

Initially, we shall proceed under the implicit assumption that all digital sampling and arithmetic operations are perfect; i.e., we ignore the effects of sampling rate and quantization noise. We defer consideration of these very important problems to a later time.

We have assumed the antenna beam to be circularly symmetric. We define $G(\beta)$ to be the antenna power gain at angle β off peak gain. We do not yet specify the form of $G(\beta)$. In Fig. 3 is depicted the conical-scan geometry. We initially assume that the antenna boresight is θ radians

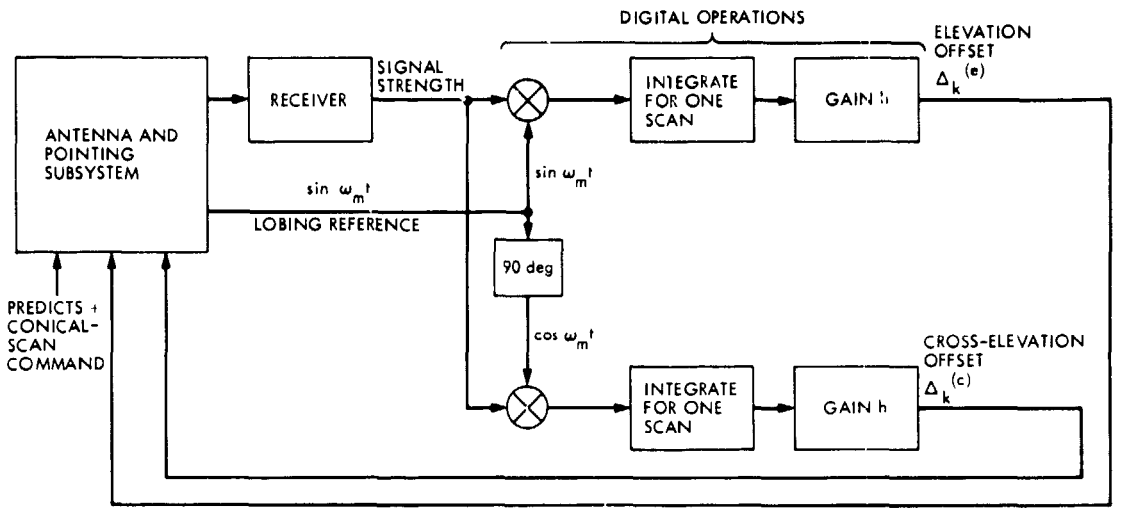

Fig. 2. System block diagram

away from the source in the cross-elevation axis and ϕ radians away from the source in the elevation axis. The conical-scan pattern is also shown in Fig. 3 as a circle of radius R, henceforth called the scan radius.

We will now calculate the error signal which the angular error (θ,ϕ) generates. The instantaneous antenna (peak gain) pointing position (θ',ϕ') is given by

$$\theta' = \theta + R\cos\omega_m t \tag{1}$$

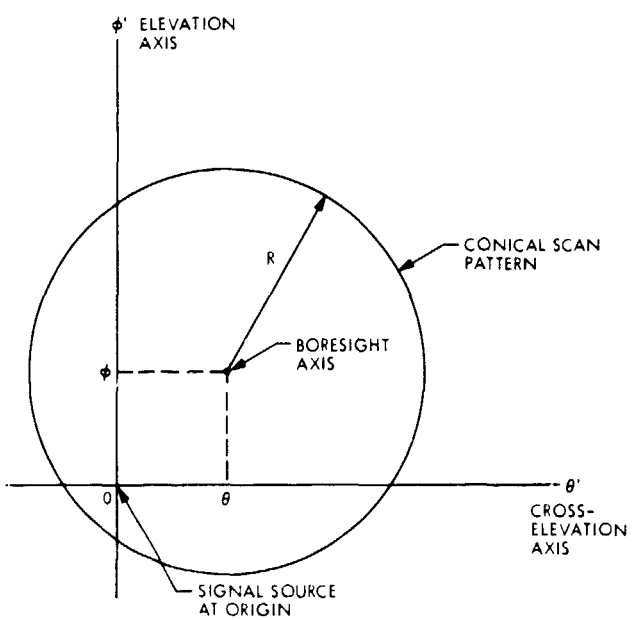

Fig. 3. Conical-scan geometry

$$\phi' = \phi + R\sin\omega_m t \tag{2}$$

where ω_m is the conical-scan rate in radians/second. This scanning is generated by the computer.

We assume the source to be, at the origin, $\theta' = 0 = \phi'$. Therefore, the instantaneous angle by which the antenna's peak gain is away from the source is, by the Pythagorean theorem, for small θ' and ϕ',

$$\beta = \sqrt{(\theta')^2 + (\phi')^2} \tag{3}$$

and, by Eqs. (1) and (2),

$$\beta = \sqrt{R^2 + \theta^2 + \phi^2 + 2R(\theta\cos\omega_m t + \phi\sin\omega_m t)} \tag{4}$$

We assume that θ and ϕ (the errors) are much smaller than R since this will be the case in practice and we can drop the θ^2 and ϕ^2 terms.

We thus obtain

$$\beta = \sqrt{R^2 + 2R\theta\cos\omega_m t + 2R\phi\sin\omega_m t} \tag{5}$$

Now again since θ and ϕ are $\ll R$, we have $R\theta \ll R^2$ and $R\phi \ll R$, and since $|\cos\omega_m t|$ and $|\sin\omega_m t|$ are ≤ 1, we can use

$$\sqrt{1+x} \approx 1 + \frac{x}{2}$$

and have

$$\beta = R + \theta\cos\omega_m t + \phi\sin\omega_m t \tag{6}$$

Now the instantaneous gain in the direction of the target as a function of time $G(t)$ is $G[\beta(t)]$ so by expanding $G(\beta)$ in a Taylor's Series around $\beta = R$ we have

$$G(t) = G(R) + G'(R)\theta\cos\omega_m t$$

$$G'(R)\phi\sin\omega_m t \tag{7}$$

where

$$G'(R) = \left.\frac{dG(\beta)}{d\beta}\right|_{\beta=R} \tag{8}$$

For simplicity we take $G'(R)$ as a positive number when $R>0$ even though it is actually negative. We have thus obtained an expression for the system gain in the target direction as a function of time in terms of the angular errors θ and ϕ in orthogonal coordinates. Note that when $\theta=0=\phi$ that $G(t)$ is constant as one expects when lobing around the target at constant offset.

III. Radio Source Tracking

We now wish to consider the performance of the conical-scan tracker on a point radio source. We assume a conventional total-power radiometer following the antenna as in Fig. 4. We take the system operating temperature to be T_{OP} and take T_S to be the radio source temperature when seen with the beam peak gain (i.e., conventional radiometry without conical-scanning). The radio source temperature seen when the source is on the conical-scan boresight is clearly

$$T_S' = \frac{G(t)}{G(0)} T_S \tag{9}$$

where $G(0)$ is the peak gain of the beam. In Fig. 4 we lump all RF and IF filtering into the voltage transfer function $H(f)$. We follow this by the conventional square-law detector and a fast lowpass resistor-capacitor (RC) filter. At this point we take the signal strength to the conical-scan circuitry (actually the computer). After the fast RC filter we also allow a conventional smoothing filter for radiometer smoothing. The fast RC filter is chosen to have a time constant no more than 1/20 of the

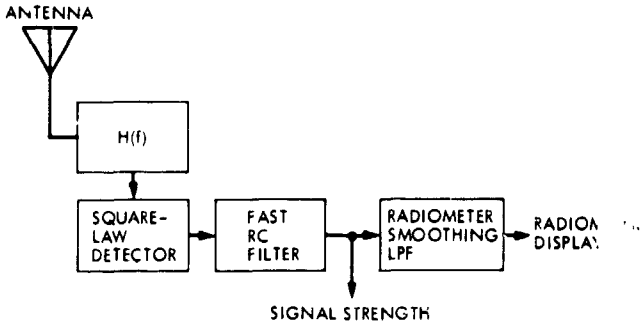

Fig. 4. Radiometer configuration

conical-scan period so that little amplitude and phase degradation of the error signal sinusoid results. If the radiometer smoothing lowpass filter (LPF) has a time constant satisfying this requirement, then the signal strength can be taken at the normal radiometer output. However, if the radiometer smoothing time approaches the conical-scan period, a fast RC filter must be used or severe performance degradation will result because the sinusoidal error signal will be smoothed out. In Chapter IV, the filtering caused by AGC is examined in detail. The results there are applicable here as well if the fast RC is not fast enough.

From Eqs. (9) and (7) the system total (instantaneous) temperature input is

$$T_i = T_{OP} + T_S\frac{G(t)}{G(0)} \tag{10a}$$

$$= T_{OP} + T_S g(R)$$

$$+ T_S g'(R)[\theta\cos\omega_m t + \phi\sin\omega_m t] \tag{10b}$$

where we have now introduced the normalized gain

$$g(\beta) = G(\beta)/G(0)$$

and its derivative

$$g'(\beta) = G'(\beta)/G(0)$$

The output of the square-law detector is

$$x(t) = CT_i B + n(t) \tag{11}$$

where B is the effective bandwidth given by

$$B = \frac{\left[\int_0^\infty |H(f)|^2 df\right]^2}{\int_0^\infty |H(f)|^4 df} \tag{12}$$

where $|H(f)|^2$ is power gain and C is just a constant representing the receiver gain (Ref. 4). The random process $n(t)$ has effectively a (two-sided) white power spectrum in watts/Hz given by

$$S_n(f) = C^2 T_i^2 B = C^2 \left[T_{OP} + T_S g(R) \right]^2 B \tag{13}$$

where θ and ϕ are assumed zero in Eq. (10b) to get this last result since they are very small and C is the same as in Eq. (11). We may assume $n(t)$ to be a Gaussian random process.

Using Eqs. (10b) and (11) we have

$$x(t) = CB\left[T_{OP} + T_S g(R) \right]$$

$$+ CBT_S g'(R)\left[\theta \cos \omega_m t + \phi \sin \omega_m t\right] + n(t) \tag{14}$$

To develop the elevation axis offset for each scan we form

$$\Delta_k^{(e)} = -h \int_0^P x(t) \sin \omega_m t \, dt \tag{15}$$

where h is a selectable gain, the e superscript on Δ denotes elevation axis, and the subscript k denotes the offset that is generated by the k^{th} scan. We have also defined the conical-scan period

$$P = 2\pi/\omega_m$$

We similarly develop the cross-elevation offset as

$$\Delta_k^{(c)} = -h \int_0^P x(t) \cos \omega_m t \, dt \tag{16}$$

We choose the same gain h for both axes, as there seems to be no advantage in having different gains. Because we are integrating over exactly one period of periodic functions it is easy to see that

$$\Delta_k^{(e)} = -h\left[A\phi_k + N_k^{(e)} \right] \tag{17}$$

and

$$\Delta_k^{(c)} = -h\left[A\theta_k + N_k^{(c)} \right] \tag{18}$$

where we have subscripted θ and ϕ to indicate their values during the k^{th} scan. Also,

$$A = CBT_S g'(R) P/2 \tag{19}$$

and

$$N_k^{(e)} = \int_0^P n(t) \sin \omega_m t \, dt \tag{20}$$

$$N_k^{(c)} = \int_0^P n(t) \cos \omega_m t \, dt \tag{21}$$

The parameter A is readily measured by observing the result of the integrals in Eqs. (15) and (16) when the system (in open-loop operation) has deliberate errors θ and ϕ.

In the Appendix it is shown that $N_k^{(e)}$ and $N_k^{(c)}$ are zero-mean random variables with common variance

$$\sigma_N^2 = \text{Var}\left[N_k^{(e)} \right] = \text{Var}\left[N_k^{(c)} \right] = C^2 \left[T_{OP} + T_S g(R) \right]^2 BP/2 \tag{22}$$

A. Dynamics of the Tracker

We now consider the dynamic performance of the conical-scan tracker. The boresight position of the tracker has been denoted by θ_k and ϕ_k, where the index k indicates their values during the k^{th} scan. We have assumed the target to be at the origin. The dynamical equations then take the difference equation form

$$\phi_{k+1} = \phi_k + \Delta_k^{(e)} \qquad \text{(elevation)} \tag{23}$$

$$\theta_{k+1} = \phi_k + \Delta_k^{(c)} \qquad \text{(cross-elevation)} \tag{24}$$

where $\Delta_k^{(e)}$ and $\Delta_k^{(c)}$ are the offsets calculated above, which are generated by the k^{th} scan. We now will consider the elevation dynamics only and will later apply the results to the cross-elevation case as well. From Eqs. (17) and (22) we see that the mean and variance of $\Delta_k^{(e)}$ are

$$E\left[\Delta_k^{(e)}\right] = -hA\phi_k \tag{25}$$

$$\mathrm{Var}\left[\Delta_k^{(e)}\right] = h^2\sigma_N^2 \tag{26}$$

From Eq. (23) and Using Eqs. (25) and (26) we can write

$$\phi_{k+1} = r\phi_k + n_k^{(e)} \tag{27}$$

where we define the decay factor r as

$$r = 1 - hA \tag{28}$$

and

$$E\left[n_k^{(e)}\right] = 0 \tag{29}$$

$$\mathrm{Var}\left[n_k^{(e)}\right] = \mathrm{Var}\left[\Delta_k^{(e)}\right] = h^2\sigma_N^2 \tag{30}$$

The equation in (27) is a first-order linear difference equation with constant coefficients. As such, we could obtain a complete solution but only two characteristics are needed here: (1) response time of the tracker (note that it will usually be much longer than the scan period), and (2) steady state tracking error.

Ignoring $\Delta_k^{(e)}$, the solution of Eq. (23) for an initial offset ϕ_1 is

$$\phi_k = r^{k-1}\phi_1 \tag{31}$$

The decay factor r determines the speed and nature of the response of the closed-loop tracker. In Table 1 is summarized the behavior of the conical-scan tracker for various values of r. We have assumed that the noise term in Eq. (23), $\Delta_k^{(e)}$, is zero, but when the system signal-to-noise ratio (SNR) is high the actual system behavior will be very similar to this noiseless case here. In Figs. 5(a) to 5(g) are depicted typical responses for each case in Table 1, where we assume an error of one unit to exist during the first scan. From the figures it is clear that cases *a*, *b*, *f*, and *g* are of no value since the error does not diminish. Although cases *c* and *e* both can converge absolutely at the same rate if the absolute values of r are equal, we will see later that case *c* will have smaller error due to noise than will case *e*. Therefore, case *e* is of no value and we are left only with cases *c* and *d* as being of use. Case *d* can be used only when the system SNR is high enough so that the error can be accurately corrected in one scan.

We shall hencefc th assume that $0 \leq r < 1$ unless specified otherwise. When r is near unity (say 0.7–0.9) the

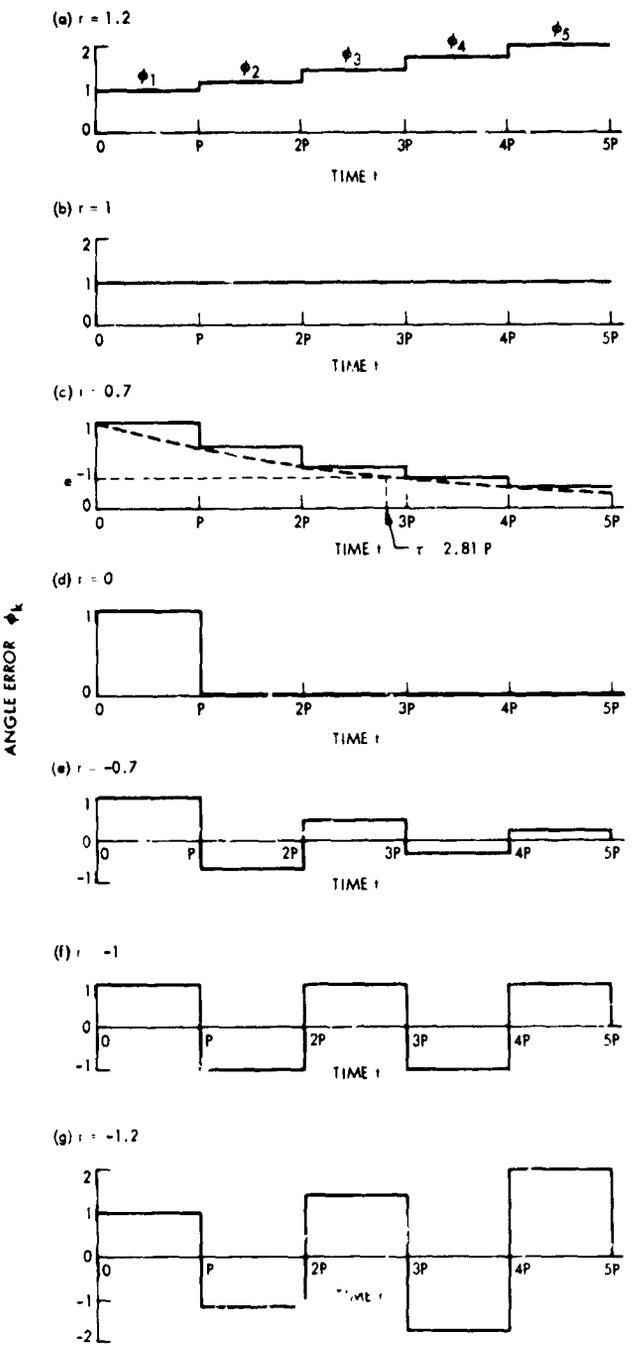

Fig. 5. Tracking responses

Table 1. Tracking response characteristics

Case	Value of r	Noiseless response	Example
a	$r>+1$	Monotonic divergence	Fig. 5a
b	$r=+1$	Constant value	Fig. 5b
c	$0<r<+1$	Monotonic convergence (useful case)	Fig. 5c
d	$r=0$	Converges in one scan (sometimes useful)	Fig. 5d
e	$-1<r<0$	Oscillatory convergence	Fig. 5e
f	$r=-1$	Constant amplitude oscillation	Fig. 5f
g	$r<-1$	Oscillatory divergence	Fig. 5g

response in Eq. (31), while discontinuous, is reasonably well approximated by an exponential decay. It is then convenient to describe the system's response characteristic in terms of a time constant of an equivalent RC circuit. A value of r near unity corresponds to having the system time constant larger than the conical-scan period P. When r is much smaller than unity, the response in Eq. (31) is very discontinuous but a proper interpretation still allows a time constant to be defined. To determine the time constant, we shall first define k_0 as the number of scans necessary to reduce ϕ_1 in Eq. (31) by $1/e$. Thus, noting that $k-1$ in Eq. (31) is the number of scans to obtain ϕ_k, we have from Eq. (31) the equation to solve for k_0

$$\phi_1/e=r^{k_0}\phi_1 \tag{32}$$

Thus

$$-1=k_0\log_e r \tag{33}$$

and

$$k_0=-1/\log_e r \tag{34}$$

Note that k_0 only fortuitously will be an integer. We now define the system time constant τ as the amount of time corresponding to k_0 conical-scan periods

$$\tau \triangleq k_0P=-P/\log_e r \tag{35}$$

For future reference we solve Eq. (35) for r

$$r=\exp(-P/\tau) \tag{36}$$

In Fig. 5(c) we show how the discrete steps match up with the exponential shape to define τ for the case $r=0.7$. We plot the exponential decay starting at (0, 1) and following the low edges of the "staircase." For small values of r the staircase steps are large, and what could be considered the average decay is $\approx P/2$ to the right. When r is small the steps are small, and the actual decay is very close to the exponential decay.

B. Performance in Noise

In Eq. (27), ϕ_k and $n_k^{(e)}$ are independent random variables since ϕ_k depends only upon $\{n_m^{(e)}, m<k\}$, which are independent of $n_k^{(e)}$ because $n(t)$ is white. Thus from Eq. (27),

$$\mathrm{Var}[\phi_{k+1}]=r^2\mathrm{Var}[\phi_k]+\mathrm{Var}[n_k^{(e)}] \tag{37}$$

We wish to find the steady state variance of ϕ_k. We do this by assuming that

$$\lim_{k\to\infty}\mathrm{Var}[\phi_k]=\sigma_\phi^2 \tag{38}$$

By taking $k\to\infty$ in Eq. (38) and using Eq. (30),

$$\sigma_\phi^2=r^2\sigma_\phi^2+h^2\sigma_N^2 \tag{39}$$

By solving for σ_ϕ^2 we have

$$\sigma_\phi^2=h^2\sigma_N^2/(1-r^2) \tag{40}$$

Solving for h from Eq. (28) and substituting in Eq. (40) gives

$$\sigma_\phi^2=\frac{(1-r)^2\sigma_N^2}{(1-r^2)A^2} \tag{41}$$

but since $1-r^2=(1+r)(1-r)$, we have

$$\sigma_\phi^2=\frac{(1-r)\sigma_N^2}{(1+r)A^2} \tag{42}$$

In Subsection A, we commented that cases *c* and *d* of Table 1 converge absolutely at the same rate if the absolute values of r are equal. We now see there is a distinct disadvantage to having $-1<r<0$. From Eq. (42), since σ_N and A do not depend on r, we see that $(1-r)/(1+r)$ is monotone decreasing over $-1<r<+1$. Therefore, although case *c* with $r=|r_0|$ and case *e* with $r=-r_0|$ will converge absolutely at the same rate, the variance of the

error in Eq. (42) is much larger for case e when r_0 is not near zero.

Using Eqs. (19) and (22) in Eq. (42) gives

$$\sigma_\phi = \left[\frac{T_{OP} + T_S g(R)}{T_S g'(R)}\right]\left(\frac{1-r}{1+r}\right)^{1/2}\left(\frac{2}{BP}\right)^{1/2} \tag{43}$$

We thus have the expression for the mean-square tracking error in the elevation axis. In Eq. (43) the first factor is a function of the source and operating temperatures and the antenna gain pattern. The second factor is a function only of r and thus, from Eq. (36), depends upon the ratio of the time constant and scan period. The last term shows that radiometer bandwidth and scan period decrease σ_ϕ. We could use Eq. (43) in this form but we choose to express the second factor of Eq. (43) in terms of τ by using Eq. (36) and have

$$\sigma_\phi = \left[\frac{\frac{T_{OP}}{T_S} + g(R)}{g'(R)} - \right]\left(\frac{1-e^{-P/\tau}}{1+e^{-P/\tau}}\right)^{1/2}\left(\frac{2}{BP}\right)^{1/2} \tag{44}$$

The second factor in Eq. (44) is well approximated by $(P/2\tau)^{1/2}$ for large τ/P. Define the rate factor F equal to the ratio of the second factor in Eq. (44) to its approximation as

$$F = \left(\frac{1-e^{-P/\tau}}{1+e^{-P/\tau}}\right)^{1/2}\frac{1}{(P/2\tau)^{1/2}} \tag{45}$$

Substitution of $F\,(P/2\tau)^{1/2}$ for the second factor in Eq. (44) gives

$$\sigma_\phi = \left[\frac{\frac{T_{OP}}{T_S} + g(R)}{g'(R)}\right]\frac{F}{\sqrt{B\tau}} \tag{46}$$

A plot of F is given in Fig. 6 and it is seen that, except for very small τ/P, F is a second-order correction to account for the lobing rate vs time constant.

It is anticipated that τ will be equal to at least a few times P. Thus we may take $F=1$ for $\tau/P \geq 2$ and have the useful result

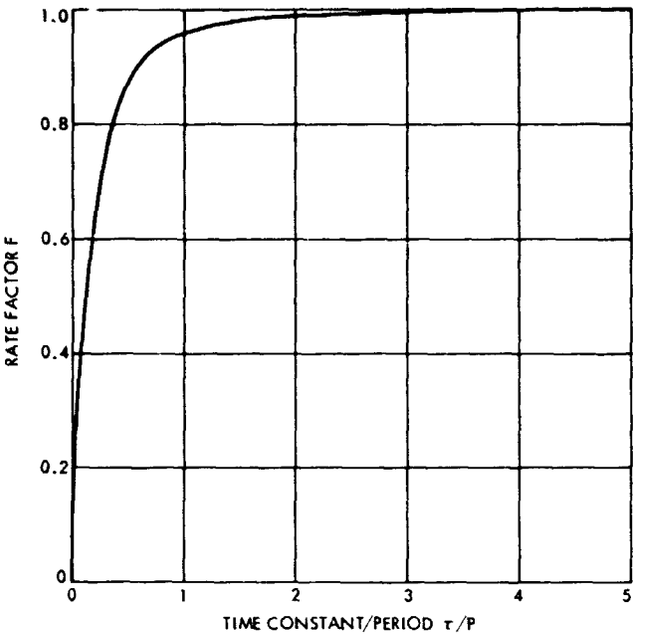

Fig. 6. Rate factor

$$\sigma_\phi = \frac{\frac{T_{OP}}{T_S} + g(R)}{g'(R)}\frac{1}{\sqrt{B\tau}} \tag{47}$$

If τ/P is not ≥ 2, Eq. (46) should be used with F taken from Fig. 6.

We now have σ_ϕ, which is the standard deviation (rms) value of the elevation angle error of the conical-scan tracker. The dimension of σ_ϕ is the same unit used in calculating $g'(R)$, i.e., normalized power gain per *degree* or per *radian*.

The results in Eqs. (46) and (47) are very general and apply for any value of R. We may now optimize the tracker by finding the value of R which minimizes σ_ϕ (holding everything else fixed). Since R enters Eq. (46) only in the first factor, we need only to minimize this factor. A special case of very great interest occurs when $T_S \ll T_{OP}$. We may then ignore $g(R)$ in Eq. (46) since it is ≤ 1. Thus, σ_ϕ is minimized when R is chosen where $g'(R)$ is maximized, i.e., where the beam pattern has the greatest slope. Remember, of course, this must be calculated from a plot of $g(R)$ with power gain presented linearly and *not* in dB.

In general, we may find R to minimize the first factor in Eq. (46) by differentiating it with respect to R and setting

the result equal to zero. The result is the following equation which must be solved for R

$$[g'(R)]^2=\left[\frac{T_{OP}}{T_S}+g(R)\right]g''(R) \tag{48}$$

A graphical argument can show that if $g(R)$ is monotonic decreasing for $R>0$, the solution of Eq. (48) gives an R greater than or equal to the value which maximizes $g'(R)$. When optimization of pointing accuracy is paramount one would choose R as above. However, there are other considerations, prime among them, the crossover loss $g(R)$. When the system is operating primarily for radiometric purposes the system ΔT_{min} will be increased by $1/g(R)$. We shall shortly consider this tradeoff in detail for a Gaussian beam pattern.

A second point is the conical-scan rate. When R is increased, the scan rate must be reduced so that mechanical stresses remain acceptable. According to Eq. (46), an increase in P has no first-order effect on σ_ϕ. However, one effect we have not yet considered is system gain fluctuation. The slower we lobe the beam the more we are susceptible to gain fluctuation errors. The analog to a Dicke radiometer is clear, whereby we wish to "switch" (rotate) faster than the gain fluctuations.

C. Performance Tradeoff

Solution of Eq. (48) is probably only of academic interest since, in practice, a tradeoff of performance vs $g(R)$ will have to be made. Probably the most useful thing we can do here is to calculate σ_ϕ as a function of R, T_{OP}, T_S, B and τ and give the tradeoff vs $g(R)$. When this is done, the solution of Eq. (48) can be taken directly from a graph, if desired. Use of an exact $g(R)$ for the antenna in question would be ideal. However, the main lobe of most antennas is approximated quite well by a Gaussian gain pattern. We shall thus assume the normalized beam power gain pattern to be

$$g(\beta)=\exp\left[-\mu(\beta/W)^2\right] \tag{49}$$

where W is the antenna beamwidth between half-power points (with the same unit as R) and

$$\mu=4\log_e 2=2.773 \tag{50}$$

We now assume that $\tau/P\geq 2$, so we may use Eq. (47). Thus, keeping only the magnitude of $g'(R)$,

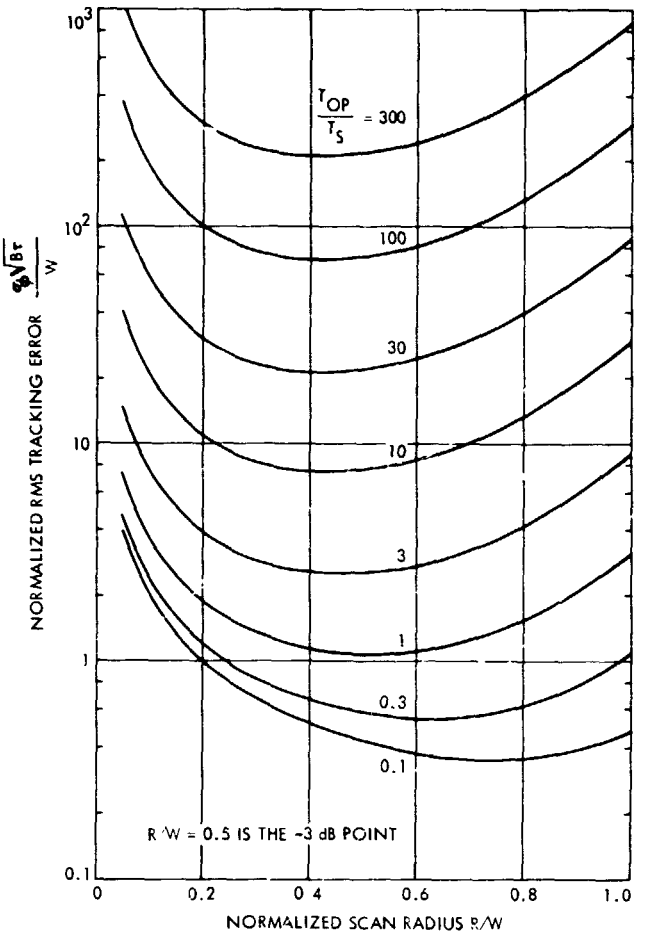

Fig. 7. Angular tracking error for radio source, gain fluctuations ignored

$$\sigma_\phi=\left[1+\frac{T_{OP}}{T_S}e^{\mu(R/W)^2}\right]\frac{W^2}{2\mu R\sqrt{B\tau}} \tag{51}$$

Normalization of σ_ϕ and use of Eq. (50) allow us to plot this relationship as

$$\boxed{\frac{\sigma_\phi\sqrt{B\tau}}{W}=(0.180)\frac{1+\dfrac{T_{OP}}{T_S}e^{2.773(R/W)^2}}{R/W}} \tag{52}$$

This is the major result for the standard deviation of the elevation error of the conical-scan tracker. The units of σ_ϕ, R and W must be the same. By symmetry, this result must also apply for the cross-elevation axis. In Fig. 7 we portray the rms angular error of Eq. (52) in terms of R/W and T_{OP}/T_S. Note carefully that $R/W=0.5$ corresponds

to the half-power point of the antenna beam. The system crossover loss is the system gain on boresight vs the antenna beam peak gain. From Eqs. (49) and (50) it is easy to show that the crossover loss in dB for a Gaussian beam is

$$g(R) \text{ in dB} = 12.04(R/W)^2 \tag{53}$$

We show this degradation in Fig. 8 so that the tradeoff of tracking error in Fig. 7 and crossover loss can be seen.

In Fig. 7 it is easy to see the values of R/W which minimize $\sigma_\phi\sqrt{B\tau}\,/W$ for fixed values of T_{OP}/T_S. When $T_{OP}/T_S \gg 1$, simple calculus shows that $g'(R)$ is maximized and hence σ_ϕ is minimized for

$$R/W = 1/\sqrt{2\mu} = 0.425 \tag{54}$$

From Fig. 7 this approximation for the minimum point is seen to hold very well down to at least $T_{OP}/T_S = 10$.

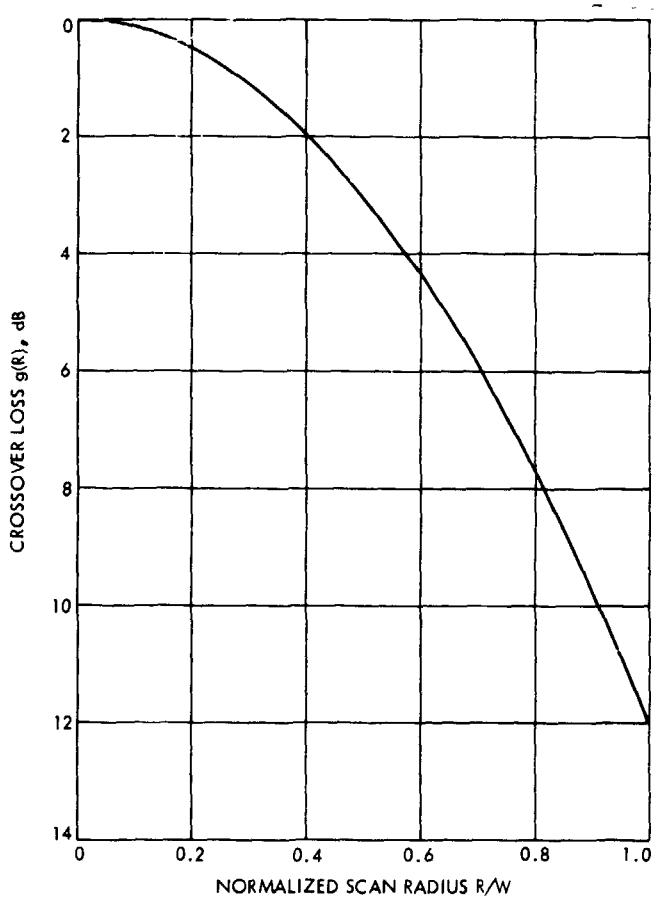

Fig. 8. Crossover loss

The derivation above of σ_ϕ has not included system gain fluctuations. Just as in Dicke-type radiometers, if the switching rate (here we have rotation rate) is not faster than the gain fluctuations, the performance will be limited by gain fluctuations. It is anticipated that scan periods of 10–100 seconds are too slow to overcome the gain fluctuations. Thus, the result of Eq. (52) is optimistic, especially for large values of the scan period P. In Section V of this analysis we shall treat gain fluctuations in the systems of interest.

It should be noted that σ_ϕ as we have derived it applies to each antenna angle axis. The errors in these axes can be assumed to be independent so the total instantaneous angle tracking error (radially) is

$$\epsilon = \sqrt{\theta^2 + \phi^2} \tag{55}$$

Because $n(t)$ is a Gaussian process, θ and ϕ are Gaussian since the system is linear. Thus the radial tracking error ϵ is a Rayleigh random variable with probability density function

$$P(\epsilon) = \begin{cases} \dfrac{\epsilon}{\sigma_\phi^2} \exp\left(-\dfrac{\epsilon^2}{2\sigma_\phi^2}\right), & \epsilon \geq 0 \\ 0 & \epsilon < 0 \end{cases} \tag{56}$$

The average radial error between boresight and target thus is

$$\bar{\epsilon} = E[\epsilon] = \int_0^\infty \epsilon p(\epsilon) d\epsilon = (\pi/2)^{1/2}\sigma_\phi = 1.25\sigma_\phi \tag{57}$$

D. Operational Considerations

To operate the system considered here, various choices of τ (or equivalently r) must be selectable. From Eqs. (35) and (28) we have

$$\tau = -P/\log_e(1 - hA) \tag{58}$$

We also have A in Eq. (19),

$$A = CBT_S g'(R)P/2 \tag{59}$$

Therefore, we see that τ is determined by P, h, C, B, T_S and R (via $g'(R)$). Even if P, h, C, B and R were held fixed, we see that the system time constant is a strong function of T_S. In order to maintain constant τ for

different radio sources, the gain parameter h must vary inversely with T_S. In addition, if the scan period P, the radiometer gain C or bandwidth B, or the scan radius R change, then h must vary so that τ will stay fixed. In most tracking systems there exists an AGC loop to maintain constant tracking bandwidth over a wide range of signal levels. At present, there is no AGC loop for radiometric work, so h will have to be set according to a calibration scheme which takes each of the above parameters into account. Solving Eqs. (58) and (59) to give h for fixed τ we have

$$h = 2\,(1 - e^{-P/\tau})/CB\,T_S\,g'(R)P \tag{60}$$

Within the computer program, calculation of h is readily made when P, τ, C, B, T_S and R (assuming the program has the $g'(R)$ function) are fed in. The value of C can be measured (or adjusted to a prescribed value) by observing the radiometer output when observing the system ambient load or cold sky. The value of B is usually close to some nominal value for a particular radiometer. The value of P may be set up as an adjustable parameter or it may be fixed in the program. Thus, τ and T_S are left as variable parameters for system operation. A direct calibration to measure A of Eq. (19) for a particular source may be a convenient technique and has the advantage of checking all system parameters in one measurement. This could be done by observing the integrator outputs, Eqs. (15) and (16), when the system pointing is running on predicts plus lobing alone, with the offset loop open and deliberate known errors in θ and ϕ existing. One problem with this method, however, is in knowing θ and ϕ exactly if the exact source position is not well known.

IV. Spacecraft Tracking

In this section we will derive the performance of the conical-scan tracker when it is used on spacecraft. We shall ignore gain fluctuation effects and defer their consideration to Section V. When the antenna's peak gain is pointed at the spacecraft, we receive a carrier power of P_s watts in the antenna. This occurs as a signal voltage

$$s(t) = \sqrt{2Z_0P_s}\,\cos(\omega_0 t + \psi) \tag{61}$$

on an impedance of Z_0 ohms, at some reference point. The quantity ψ is the phase of the received signal. The lobing procedure in Section II produces the instantaneous angle β in Eq. (4) by which the antenna's peak gain is away from the spacecraft. We assume the antenna gain pattern to be well approximated by a Gaussian shape as in Eq. (49). The normalized antenna voltage gain is thus, by square-rooting (Eq. 49),

$$v(\beta) = \exp\left[-\mu'(\beta/W)^2\right] \tag{62}$$

where

$$\mu' = \mu/2 = 1.387$$

The normalized voltage gain vs time is, from Eqs. (4) and (62),

$$\begin{aligned} v(t) &= v[\beta(t)] \\ &= \exp\left\{-\frac{\mu'}{W^2}\left[R^2 + \theta^2 + \phi^2 \right.\right. \\ &\quad \left.\left. + 2R(\theta\cos\omega_m t + \phi\sin\omega_m t)\right]\right\} \end{aligned} \tag{63}$$

We then see that the signal voltage received when the antenna is conically scanned is

$$r(t) = v(t)s(t) \tag{64}$$

At the point where we define signal power we also define the system operating temperature T_{OP} which gives

$$N_0 = kT_{OP}\ \text{watts/Hz} \tag{65}$$

on Z_0 ohms, where k is Boltzmann's constant.

Without loss of generality we may take $Z_0 = 1$ ohm and then the received signal plus noise is

$$r(t) = v(t)\sqrt{2P_s}\cos(\omega_0 t + \psi) + n(t) \tag{66}$$

where $n(t)$ has the two-sided power spectral density

$$S_n(f) = N_0/2 \tag{67}$$

A. Manual Gain Control

We shall first consider conical-scan tracking when the receiver AGC is not used and the receiver gain is fixed. We treat this case for two reasons: (1) it can be solved exactly and provides a jumping-off point for the approximate analysis of the AGC case and (2) when the

AGC is faster than the scan rate the manual gain control (MGC) result will apply.

We must detect the amplitude of the signal in Eq. (66) so that we may correlate with $\sin\omega_m t$ and $\cos\omega_m t$ to give pointing information. Coherent detection is accomplished in a phase detector used for AGC detection by means of a reference signal generated by the phase-locked loop (PLL). The PLL tracks the phase ψ of the signal and generates a reference signal

$$v_{ref}(t)=\sqrt{2}\cos(\omega_0 t+\hat{\psi}) \tag{68}$$

where $\hat{\psi}$ is the PLL's estimate of ψ. We ignore heterodyning and equivalently assume the PLL to be generating its reference in the RF range. The phase detector forms

$$y(t)=v_{ref}(t)r(t) \tag{69}$$

Ignoring double-frequency terms we have

$$y(t)=v(t)\sqrt{P_s}\cos(\psi-\hat{\psi})+n'(t) \tag{70}$$

where $n'(t)$ is again a white process with power spectral density (Ref. 5)

$$S_{n'}(f)=N_0/2 \tag{71}$$

If the PLL loop SNR is above about 6 dB. $\hat{\psi}$ is close enough to ψ that $\cos(\psi-\hat{\psi})\approx 1$. We assume this to be the case here. If the PLL is operating nearer than 6 dB to threshold this approximation will be optimistic. We thus have

$$y(t)\approx v(t)\sqrt{P_s}+n'(t) \tag{72}$$

Because of receiver gains the actual signal presented at the signal strength point in Fig. 2 will be different by some gain K over Eq. (72). Including this in Eq. (72) we have the signal strength $x(t)$

$$x(t)=K\left[v(t)\sqrt{P_s}+n'(t)\right] \tag{73}$$

We now use Eqs. (15) and (16) to develop the offsets for the elevation and cross-elevation axes. We start with elevation and have

$$\Delta_k^{(e)}=-h\left[K\sqrt{P_s}\,d_k+N_k^{(e)}\right] \tag{74}$$

where

$$d_k=\int_0^P v(t)\sin\omega_m t\,dt \tag{75}$$

$$N_k^{(e)}=K\int_0^P n'(t)\sin\omega_m t\,dt \tag{76}$$

For simplicity, these integrations are tacitly assuming a time scale starting at $t=0$ at the beginning of each scan. From Eqs. (63) and (75),

$$d_k=\exp\left[-\frac{\mu'}{W^2}(R^2+\theta_k^2+\phi_k^2)\right]$$

$$\times\int_0^P \sin\omega_m t\exp\left[-\frac{\mu R}{W^2}(\theta_k\cos\omega_m t+\phi_k\sin\omega_m t)\right]dt \tag{77}$$

The exponential under the integral can be rewritten as

$$\exp[-\xi_k\cos(\omega_m t-\lambda_k)] \tag{78}$$

where

$$\xi_k=\mu R\sqrt{\theta_k^2+\phi_k^2}\,/W^2 \tag{79}$$

and

$$\lambda_k=\tan^{-1}\left(\frac{\phi_k}{\theta_k}\right) \tag{80}$$

The Jacobi–Anger formula is (Ref. 6)

$$\exp(\xi\cos\beta)=I_0(\xi)+2\sum_{n=1}^{\infty}I_n(\xi)\cos n\beta \tag{81}$$

where $I_n(\xi)$ is the modified Bessel function of the first kind. We may expand Eq. (78) using Eq. (81) and obtain

$$\exp[-\xi_k\cos(\omega_m t-\lambda_k)]$$

$$=I_0(-\xi_k)+2\sum_{n=1}^{\infty}I_n(-\xi_k)\cos[n(\omega_m t-\lambda_k)] \tag{82}$$

Use of this in Eq. (77) gives only the following term since, for $n \neq 1$, the sinusoids in Eq. (82) are orthogonal to $\sin \omega_m t$:

$$d_k = \exp\left[-\frac{\mu'}{W^2}(R^2 + \theta_k^2 + \phi_k^2) \right] 2I_1(-\xi_k)$$

$$\times \int_0^P \sin \omega_m t \cos(\omega_m t - \lambda_k) dt \tag{83}$$

$$d_k = PI_1(-\xi_k) \sin\lambda_k \exp\left[-\frac{\mu'}{W^2}(R^2 + \theta_k^2 + \phi_k^2) \right] \tag{84}$$

From Eq. (80) we see

$$\sin\lambda_k = \phi_k / \sqrt{\theta_k^2 + \phi_k^2} \tag{85}$$

Also

$$I_1(-x) = -I_1(x) \tag{86}$$

Thus

$$d_k = -\phi_k P \frac{I_1\left(\frac{\mu R}{W^2} \sqrt{\theta_k^2 + \phi_k^2} \right)}{\sqrt{\theta_k^2 + \phi_k^2}} \exp\left[-\frac{\mu'}{W^2}(R^2 + \theta_k^2 + \phi_k^2) \right] \tag{87}$$

The result in Eq. (87) is exact, but is more precise than needed.[1] We may simplify this result with essentially no loss in accuracy. Note that

$$\sqrt{\theta_k^2 + \phi_k^2}$$

is the radial error. This error will generally be much smaller than W. Also, R will be less than or comparable to W. Therefore the argument of I_1 in Eq. (87) will be much smaller than unity and we may use the first term of the power series expansion of $I_1(x)$,

$$I_1(x) \approx x/2 \tag{88}$$

Using this, Eq. (87) becomes

$$d_k = -\phi_k \frac{P\mu R}{2W^2} \exp\left[-\frac{\mu'}{W^2}(R^2 + \theta_k^2 + \phi_k^2) \right] \tag{89}$$

Further, we assume $|\theta_k|$ and $|\phi_k|$ to be $\ll R$. We then may neglect θ_k and ϕ_k in the exponential and we have

$$d_k = -\phi_k \frac{P\mu R}{2W^2} \exp\left[-\mu'(R/W)^2 \right] \tag{90}$$

This last approximation will be valid unless R is chosen very small and σ_θ and σ_ϕ are comparable to R.

From Eqs. (74) and (90) we have

$$\Delta_k^{(e)} = -h\left[A\phi_k + N_k^{(e)} \right] \tag{91}$$

where

$$A = \frac{KP\mu R\sqrt{P_s}}{2W^2} \exp\left[-\mu'(R/W)^2 \right] \tag{92}$$

We dropped the minus sign in Eq. (90), so the correction is in the right direction. In Eq. (91) we have the same equation as Eq. (17). We need only find the variance of $N_k^{(e)}$ and we shall be able to directly use Subsections A and B of Section III to find performance.

We know $N_k^{(e)}$ has zero mean because $n'(t)$ is white. Also in the Appendix we substitute $Kn'(t)$ for $n(t)$ and obtain

$$\sigma_N^2 = K^2 \int_0^P \int_0^P R_{n'}(t_1 - t_2) \sin \omega_m t_1 \sin \omega_m t_2 \, dt_1 \, dt_2 \tag{93}$$

Since $n'(t)$ has the power spectral density in Eq. (71) we know

$$R_{n'}(t_1 - t_2) = \frac{N_0}{2} \delta(t_1 - t_2) \tag{94}$$

[1] In Section III, linearization was assumed first and then a Gaussian beam. Here a Gaussian beam was assumed first and now linearization is to be done. Either sequence could be used in either place—the result is the same.

Use of Eq. (94) in Eq. (93) gives

$$\sigma_N^2 = PK^2N_0/4 \tag{95}$$

We now can use Subsection A of Section III in its entirety for the spacecraft case. We may also use Subsection B through Eq. (42) and the paragraph immediately following it. Upon substitution of Eqs. (92) and (95) in Eq. (42) we have

$$\sigma_\phi = \left(\frac{1-r}{1+r}\right)^{\frac{1}{2}} \frac{W^2\sqrt{N_0}\,\exp\left[\mu'(R/W)^2\right]}{\sqrt{P}\,\mu R\sqrt{P_s}} \tag{96}$$

Expressing r as in Eq. (36) and defining the rate factor F as in Eq. (45) we have

$$\sigma_\phi = \frac{FW^2\sqrt{N_0}\,\exp\left[\mu'(R/W)^2\right]}{\mu R\sqrt{P_s}\,\sqrt{2\tau}} \tag{97}$$

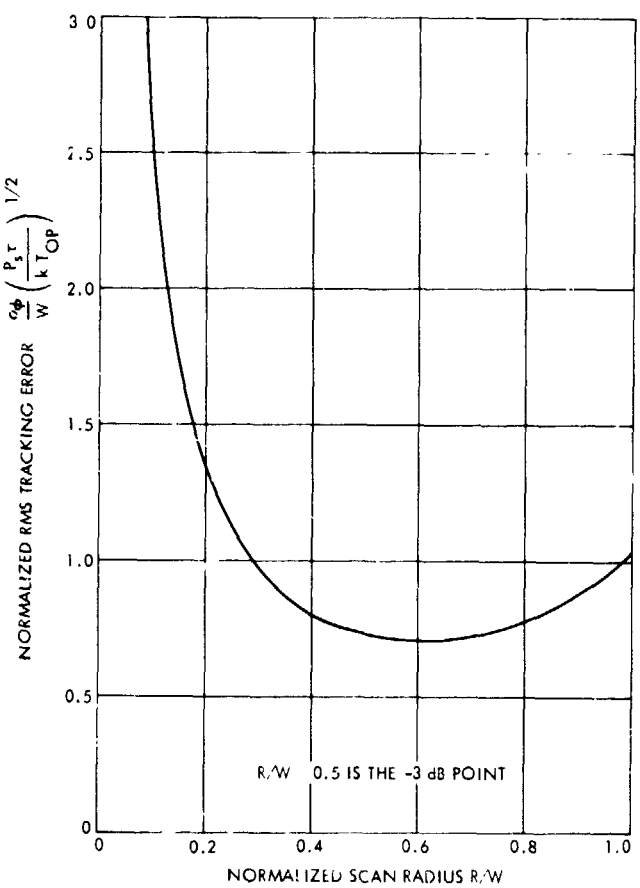

Fig. 9. Angular tracking error for spacecraft, gain fluctuations ignored

As in Section III we argue that $F \approx 1$ for practical applications. Also by use of Eq. (65) we obtain

$$\sigma_\phi = \frac{W^2\sqrt{kT_{OP}}\,\exp\left[\mu'(R/W)^2\right]}{\mu R\sqrt{P_s}\,\sqrt{2\tau}} \tag{98}$$

Normalization and putting in the values of μ and μ' give

$$\boxed{\frac{\sigma_\phi}{W}\left(\frac{P_s\tau}{kT_{OP}}\right)^{1/2} = (0.255)\frac{\exp\left[1.387(R/W)^2\right]}{R/W}} \tag{99}$$

By symmetry this result also applies to the cross-elevation axis as well. This result is presented in Fig. 9. Boltzmann's constant k has been included in the normalization because it is felt that $\sqrt{P_s/kT_{OP}}$ is most easily computed using dB, whereby k is -198.6 dBmW $-$ K $-$ Hz. Note that $P_s\tau/kT_{OP}$ is dimensionless because $1/\tau$ has the dimension of hertz.

The crossover loss, which is the loss of gain on boresight vs the antenna beam peak gain, is the same as shown

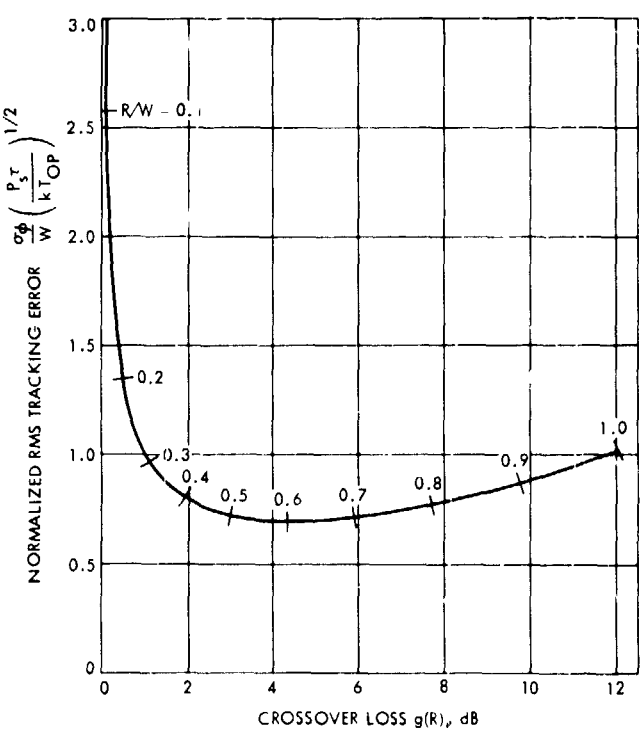

Fig. 10. Tracking error vs crossover loss, gain fluctuations ignored

in Fig. 8. For ease in comparing σ_ϕ vs $g(R)$ we show their tradeoff in Fig. 10, which is a cross-plot of Figs. 8 and 9.

If all parameters are held constant except R, simple calculus shows that the minimum σ_ϕ in Eq. (83) and Fig. 9 occurs when $R=(0.601)W$. If pointing accuracy were paramount then this choice of R would be optimum unless the crossover loss of 4.3 dB given by Fig. 8 causes the phase-locked loop to approach threshold. From Fig. 10, it can be seen that permitting σ_ϕ to be only twice its minimum attainable value allows $g(R)$ to be reduced from 4.3 dB to 0.45 dB, a sizable reduction.

The reader must be cautioned that gain fluctuation effects have not been included in this calculation but will be considered in Section V. The present result is sufficient to characterize performance as long as the conical-scan rate is faster than the gain fluctuations.

B. Automatic Gain Control

To maintain signal levels in the PLL receiver near nominal values over a wide range of input signal levels, AGC is used. A secondary benefit is that of maintaining approximately constant closed loop bandwidth when performing a tracking function such as monopulse pointing or linear polarization tracking. This advantage also occurs in the conical-scan tracker. However, it is a mixed blessing since the choice of AGC speed will often not be made to optimize pointing but to optimize PLL locking performance. If the AGC is very slow the error signal we develop by conical-scan tracking will be attenuated and phase-shifted by the AGC circuitry. Let us begin by considering the AGC characteristic with respect to the steady component of signal level (ignoring temporarily the small sinusoidal error signal). It is known that the dynamic AGC voltage of the PLL receivers used is very close to -1.0 V over a signal range of better than 60 dB. Thus it is clear that the receiver gain must vary inversely as the signal voltage. Thus, when using AGC the K in Eq. (73) will actually be

$$K=K'/\left\{\sqrt{P_s}\exp\left[-\mu'(R/W)^2\right]\right\} \tag{100}$$

where K' is a fixed quantity and $\sqrt{P_s}$ is, of course, proportional to signal voltage. If the AGC response is much faster than the conical-scan rate ω_m, so that the AGC gain at frequency ω_m is the same as for the DC steady state signal component, we argue that $K=K'/\sqrt{P_s}$ also for the error signal and Eq. (92) becomes

$$A=\frac{K'P\mu R}{2W^2} \tag{101}$$

Also, from Eqs. (86) and (93), we now see that the system closed loop time constant theoretically does not depend upon the signal level P_s. This represents a distinct advantage over the conical-scan tracking of radio sources in Section III, where τ does depend upon the source temperature T_s.

The performance of the conical-scan tracker under the assumption that the AGC is much faster than ω_m is just that given in Eq. (99), since using Eq. (100) in Eq. (95) and by use of Eqs. (101) and (42) again gives Eq. (96), and everything down to Eq. (99) follows.

In practice, however, the AGC may not satisfy the criterion of being much faster than ω_m. We now consider this case. For small signal amplitude variations (applicable to the error signal) the AGC circuit acts as a single pole filter with transfer function (Ref. 7):

$$H(\omega)=\frac{b}{1+j\omega\tau_A} \tag{102}$$

where b is dc gain and τ_A is the filter response time. Note that τ_A is not the so-called "AGC filter time constant" which is $\approx$380, $\approx$34, or $\approx$4s in DSN Block III receivers. These numbers represent the time constant of an RC operational amplifier circuit approximating an integrator in the AGC loop. Since these time constants are in the feedback loop, the overall response time τ_A is determined by the open loop gain, which is a slowly varying function of signal level. To find τ_A, it is a simple matter to put a small step change in a test transmitter signal level and observe the AGC response time to $1/e$. For example, a filter time constant of 380 s generally gives a value for τ_A which is on the order of 5 s.

If $\tau_A \ll 1/\omega_m$, the effect of the AGC is nil since the error signal is affected the same as the steady signal component. This is the case we treated above. However, if τ_A increases toward $1/\omega_m$, the AGC causes attenuation and phase shift of the error signal. The apparent error signal amplitude will be diminished and the tracking response will thus be slower. This arises due directly to the AGC attenuation and indirectly to the AGC phase shift because the error signal will be out of phase with the reference signals in the correlation procedure. One way to resolve the matter is to apply analog compensation to the AGC voltage before performing the correlations. A suitable filter would be the following:

$$H_{\text{comp}}(\omega) = 1 + j\omega\tau_A \qquad (103)$$

which cancels the pole in Eq. (102). Practical implementation dictates that Eq. (103) has, in addition, a second-order high-frequency roll-off determined by the analog-to-digital sampling rate. With the compensation of Eq. (103), performance of the conical-scan tracker would be identical to that of the fast AGC case above, i.e., the MGC result in Eq. (99). The compensation in Eq. (103) can also be accomplished digitally in the computer after sampling.

A second way to remove the smoothing effect of the AGC is to apply a gain to the error signal equal to that loss caused by the AGC and apply a phase shift to the correlating reference signals equal to that caused by the AGC. If τ is several times P so the error signal changes slowly (thus looking approximately like a sine wave) the system response will be equivalent to that obtained by using the analog or digital compensation discussed above. The reason is that if the error signal looks like a sine wave with slowly varying envelope the system will be looking at the noise spectrum only for a small bandwidth $\approx 1/\tau$ around ω_m. Over this small bandwidth the AGC transfer function is approximately constant. Hence, the error signal looks like a narrowband signal plus white noise, and the effect of the AGC is equivalently a gain and phase shift at $\omega = \omega_m$. When τ and P are of comparable magnitude this argument does not hold because the error signal no longer is narrowband, and the analysis is very difficult and will not be carried out. Logic indicates, however, that the system will still work and it is felt that system performance will not significantly change from the $\tau \ll P$ case even up to $\tau = P$. Since it is anticipated that $\tau \ll P$, it is felt that an exact analysis for arbitrary τ and P is not really needed.

For ease of calculation, the attenuation and phase shift of the error signal due to the AGC are presented in Figs. 11 and 12. Gain magnitude is

$$\frac{|H(\omega_m)|}{H(0)} = 1/\sqrt{1 + (2\pi\tau_A/P)^2} \qquad (104)$$

and phase shift is

$$\text{Angle}[H(\omega_m)] = -\tan^{-1}(2\pi\tau_A/P) \qquad (105)$$

From Figs. 11 and 12 it is seen that $\tau_A/P = 0.05$ reduces the gain by only 0.95 and gives only -18 deg of phase shift. Remembering that phase error causes the output amplitude of the correlation procedure to drop as the cosine of the error, the total drop in loop gain (vs the fast AGC case) is $0.95\cos(-18\text{ deg}) = 0.90$, a small change. Thus, as long as $\tau_A/P < 0.05$ we probably do not need to worry about compensation. Note that Figs. 11 and 12 and the argument above apply equally well to the specification of the "fast" RC filter when tracking radio sources (see Section III) and was the argument used there to require that $\tau_{RC}/P < 0.05$. It should be observed that a phase error of 30 deg or more gives substantial "cross-talk" between elevation and cross-elevation axes, which results in a deterioration of performance and can produce an unstable system as the phasing error approaches 90 deg.

In conclusion, we find that the performance under AGC is the same as for MGC, namely Eq. (99), as long as we compensate for the AGC filtering action when necessary.

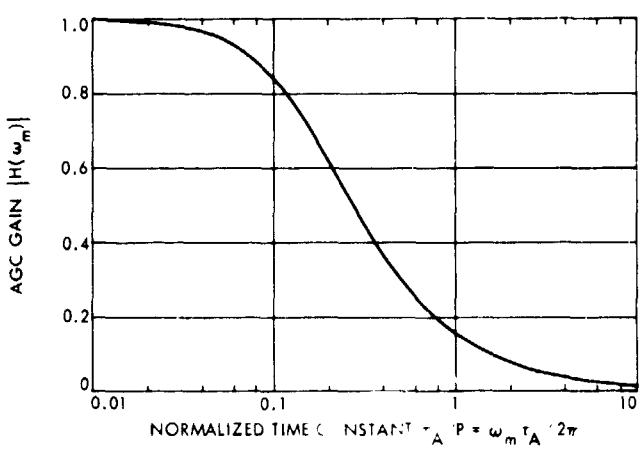

Fig. 11. AGC gain magnitude

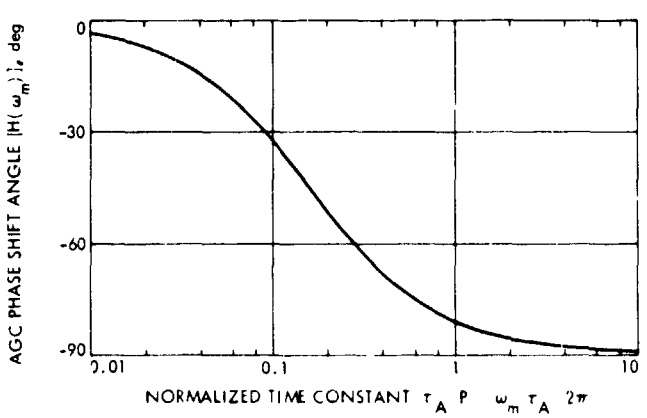

Fig. 12. AGC phase shift

V. Gain Fluctuation Effects

In Sections III and IV, the analyses of tracking performance were made under the assumption that fluctuation of the system gain was of no consequence. In a practical case, this would be justified only if the scan rate were much faster than any significant spectral component of the gain fluctuation. In this section we shall consider the gain fluctuation problem in detail.

The gain of all receiving systems varies with time. Mechanical flexure due to vibration, varying stresses, etc., and thermal variations are the well-known primary causes. Good receiver design usually can reduce the problem to an insignificant level everywhere except in active devices at RF frequencies. For DSN receiving systems, the masers are thought to be the principal contributors to gain (and also phase) instabilities. The gain stability is excellent by most standards and is satisfactory for virtually all communication purposes. However, for radiometry and the present tracking applications, the gain fluctuation of the system will be seen to give the fundamental limit for the tracking accuracy available.

We now define the receiver gain as the gain from the feed horn down to the point where we convert to digital format as

$$Q(t) = Q_0[1 + F(t)] \tag{106}$$

where $F(t)$ is the gain fluctuation. We really do not need to specify Q_0 very carefully, as it will drop out of the analysis. All we need is to realize that the system gain varies as $1 + F(t)$. For good receivers, we have

$$|F(t)| \ll 1 \tag{107}$$

Thus the voltage gain clearly varies as

$$\sqrt{1 + F(t)} \approx 1 + \frac{F(t)}{2} \tag{108}$$

We shall model $F(t)$ as a stationary random process and we assume that we have knowledge of the statistics (i.e., spectrum) of $F(t)$.

A. Tracking of Radio Sources

We start with Eq. (14) and multiply it by our time-varying gain $[1 + F(t)]$ to give $x'(t)$:

$$x'(t) = [1 + F(t)]x(t) \tag{109}$$

$$= CB[1 + F(t)][T_{OP} + T_S g(R)]$$

$$+ CB[1 + F(t)]T_S g'(R)[\theta \cos \omega_m t + \phi \sin \omega_m t]$$

$$+ [1 + F(t)]n(t) \tag{110}$$

Since $|F(t)| \ll 1$, we may neglect $F(t)$ with respect to unity in the second and third terms of Eq. (110). We may do this because in the second term $F(t)$ causes a very small random variation in closed loop bandwidth and in the third term $F(t)$ causes a very small random variation in the input noise level. Neither of these are first-order effects. In the first term of Eq. (110), $F(t)$ does cause a first-order effect, as we shall see. Upon neglecting $F(t)$ as above we find from Eq. (110) that

$$x'(t) = \Lambda F(t) + x(t) \tag{111}$$

where

$$\Lambda = CB[T_{OP} + T_S g(R)] \tag{112}$$

We now form $\Delta_k^{(s)}$ and $\Delta_k^{(c)}$ as in Eqs. (15) and (16) by substituting $x'(t)$ for $x(t)$ therein

$$\Delta_k^{(s)} = -h \int_{(k-1)P}^{kP} x'(t) \sin \omega_m t \, dt \tag{113}$$

$$\Delta_k^{(c)} = -h \int_{(k-1)P}^{kP} x'(t) \cos \omega_m t \, dt \tag{114}$$

We carefully specified the integration limits in Eqs. (113) and (114) instead of starting $t = 0$ at the beginning of each scan as in Section III because we will need to consider correlation between the values of $F(t)$ in different scans. We now will consider just the elevation axis and appeal to symmetry later. By putting Eq. (111) in Eq. (113) and integrating as in Section III, we get Eq. (17) plus an extra term which is due to the first term in Eq. (111)

$$\Delta_k^{(s)} = -h[A\phi_k + N_k^{(s)}] + m_k^{(s)} \tag{115}$$

where

$$m_k^{(s)} = -h\Lambda \int_{(k-1)P}^{kP} F(t) \sin \omega_m t \, dt \tag{116}$$

A is as in Eq. (19) and $N_k^{(e)}$ is as in Eq. (20). Starting with Eq. (17), we follow down to Eq. (30), keeping the extra term $m_k^{(e)}$ in Eq. (115) added on. We then have in analog to Eq. (27)

$$\phi_{k+1} = r\phi_k + n_k^{(e)} + m_k^{(e)} \tag{117}$$

where r and $n_k^{(e)}$ are specified in Eqs. (28–30).

Because $m_k^{(e)}$ and $m_j^{(e)}$ are not independent when $j \neq k$, we shall have to consider the actual solution of Eq. (117) rather than just evaluate variances as independence allowed us in Section III. The exact solution of Eq. (117), assuming we start at $t=0$ with $\phi = \phi_1$, is

$$\phi_k = \phi_1 r^{k-1} + \sum_{p=1}^{k-1} r^{k-p-1}\left[n_p^{(e)} + m_p^{(e)}\right] \tag{118}$$

Note that the summation term is random while the first term is just Eq. (31). Thus we see the response time characteristic is the same as in Subsection A of Section III. We are primarily concerned with the steady state variance of ϕ_k, so we take k very large. Since $|r|<1$ the first term of Eq. (118) drops out. We make the substitution $i = k-p-1$ in Eq. (118) and have

$$\phi_k = \sum_{i=0}^{k-2} r^i\left[n_{k-i-1}^{(e)} + m_{k-i-1}^{(e)}\right] \tag{119}$$

Since $n_p^{(e)}$ and $m_p^{(e)}$ are stationary, we may drop $k-1$ from the two subscripts in Eq. (119) and reverse the sign of i without any change in the statistics of ϕ_k. We then have

$$\phi_k = \sum_{i=0}^{k-2} r^i\left[n_i^{(e)} + m_i^{(e)}\right] \tag{120}$$

We desire the variance of ϕ_k as $k \to \infty$ so if we take $k \to \infty$ in Eq. (120) we have

$$\phi_\infty = \sum_{i=0}^{\infty} r^i\left[n_i^{(e)} + m_i^{(e)}\right] \tag{121}$$

The steady state variance of ϕ_k is then

$$\sigma^2 = \mathrm{Var}[\phi_\infty] = E\left[\phi_\infty^2\right]$$

$$= E\sum_{p=0}^{\infty}\sum_{i=0}^{\infty} r^{i+p}\left[n_i^{(e)} + m_i^{(e)}\right]\left[n_p^{(e)} + m_p^{(e)}\right] \tag{122}$$

$$= \sum_{p=0}^{\infty}\sum_{i=0}^{\infty} r^{i+j} E\left[n_i^{(e)}n_p^{(e)} + n_i^{(e)}m_p^{(e)} + m_i^{(e)}n_p^{(e)} + m_i^{(e)}m_p^{(e)}\right] \tag{123}$$

Now from Eqs. (28–30) and the first sentence of Subsection B of Section III,

$$E\left[n_i^{(e)}n_p^{(e)}\right] = \begin{cases} h^2\sigma_N^2 & i=p \\ 0 & i\neq p \end{cases} \tag{124}$$

and

$$E\left[n_i^{(e)}m_p^{(e)}\right] = 0 \tag{125}$$

Thus

$$\sigma^2 = h^2\sigma_N^2\sum_{i=0}^{\infty} r^{2i} + \sum_{i=0}^{\infty}\sum_{p=0}^{\infty} r^{i+p}E\left[m_i^{(e)}m_p^{(e)}\right] \tag{126}$$

The first summation is $1/(1-r^2)$ so the first term of Eq. (126) is $h^2\sigma_N^2/(1-r^2)$, which is just σ_ϕ^2 in Eq. (40). Thus the first term of Eq. (126) is just the steady state variance of ϕ_k when $F(t)=0$. We then write

$$\sigma^2 = \sigma_\phi^2 + \sigma_g^2 \tag{127}$$

where σ_g^2 is the second term of Eq (126) and is the variance due to gain fluctuations, and σ_ϕ^2 is as calculated in Section III (or Section IV when discussing spacecraft tracking later in this section).

We now need to find σ_g^2. From Eqs. (126) and (116),

$$\sigma_g^2 = h^2\Lambda^2\sum_{i=0}^{\infty}\sum_{p=0}^{\infty} r^{i+p}\int_{(i-1)P}^{iP}\int_{(p-1)P}^{pP} E\left[F(t_1)F(t_2)\right]\sin\omega_m t_1 \times \sin\omega_m t_2\, dt_1\, dt_2 \tag{128}$$

The expectation in Eq. (128) is the autocorrelation of $F(t)$

$$E\left[F(t_1)F(t_2)\right] = R_F(t_1 - t_2) \tag{129}$$

which may be expressed in terms of its power spectral density $S_F(f)$ as

$$R_F(t_1-t_2)=\int_{-\infty}^{\infty} S_F(f)e^{j2\pi f(t_1-t_2)}df \tag{130}$$

where

$$j=\sqrt{-1} \tag{131}$$

Substitution of Eqs. (129) and (130) in Eq. (128) and interchanging integrals gives

$$\sigma_g^2=h^2\Lambda^2\sum_{i=0}^{\infty}\sum_{p=0}^{\infty} r^{i+p}I_{pi} \tag{132}$$

where

$$I_{pi}=\int_{-\infty}^{\infty} S_F(f)\gamma_p(f)\gamma_i^*(f)df \tag{133}$$

where * denotes complex conjugation, and

$$\gamma_p(f)=\int_{(p-1)P}^{pP}\sin\omega_m t\, e^{-j2\pi ft}dt \tag{134}$$

Evaluation of $\gamma_p(f)$ via much algebra gives

$$\gamma_p(f)=\frac{\omega_m e^{-j2\pi fpP}(e^{j2\pi fP}-1)}{\omega_m^2-(2\pi f)^2} \tag{135}$$

Substitution of Eq. (135) into Eq. (133) gives

$$I_{pi}=4\omega_m^2\int_{-\infty}^{\infty}\frac{S_F(f)\sin^2\pi fP e^{j2\pi fP(i-p)}df}{\left[\omega_m^2-(2\pi f)^2\right]^2} \tag{136}$$

Substitution of this into Eq. (132) and rearrangement gives

$$\sigma_g^2=h^2\Lambda^2 4\omega_m^2\int_{-\infty}^{\infty}\frac{S_F(f)\sin^2\pi fP}{\left[\omega_m^2-(2\pi f)^2\right]^2}\times\sum_{i=0}^{\infty}(re^{j2\pi fP})^i\sum_{p=0}^{\infty}(re^{-j2\pi fP})^p df \tag{137}$$

The first summation is

$$\sum_{i=0}^{\infty}(re^{j2\pi fP})^i=(1-re^{j2\pi fP})^{-1} \tag{138}$$

and the second one is

$$\sum_{p=0}^{\infty}(re^{-j2\pi fP})^p=(1-re^{-j2\pi fP})^{-1} \tag{139}$$

The product of the summations can be manipulated to give $(1+r^2-2r\cos 2\pi fP)^{-1}$. We can thus rewrite Eq. (137) as

$$\sigma_g^2=h^2\Lambda^2 4\omega_m^2\int_{-\infty}^{\infty}\frac{S_F(f)\sin^2\pi fP}{\left[\omega_m^2-(2\pi f)^2\right]^2(1+r^2-2r\cos 2\pi fP)}df \tag{140}$$

Upon substituting $h=(1-r)/A$ from Eq. (28), Λ from Eq. (112) and A from Eq. (19) and using

$$f_m=\omega_m/2\pi=1/P \tag{141}$$

where f_m is the conical-scan rate in Hz, we have

$$\sigma_g^2=\left[\frac{\frac{T_{OP}}{T_S}+g(R)}{g'(R)}\right]^2\Gamma \tag{142}$$

where

$$\Gamma=\int_{-\infty}^{\infty} S_F(f)W(f)\,df \tag{143}$$

and the weighting function $W(f)$ is

$$W(f)=\frac{4(1-r)^2\sin^2(\pi f/f_m)}{\pi^2\left[1-\left(\frac{f}{f_m}\right)^2\right]^2\left[1+r^2-2r\cos(2\pi f/f_m)\right]} \tag{144}$$

By use of Eqs. (127) and (47) we obtain

$$\sigma = \left[\frac{\frac{T_{OP}}{T_S} + g(R)}{g'(R)}\right]\left(\frac{1}{B\tau} + \bar{\Gamma}\right)^{1/2} \tag{145}$$

This is the principal general result for tracking of radio sources.

It must be realized that Γ from Eq. (143) depends on r via $W(f)$ in Eq. (144) and hence upon τ, since from Eq. (35)

$$r = e^{-P/\tau} \tag{146}$$

We now wish to examine in detail how Γ depends upon τ (via r), f_m and $S_F(f)$. In Fig. 13 we plot $W(f)$ from Eq. (144) as a function of f for various values of r. It can be shown that the $W(f)$ for any $r = |r_0|$ is smaller than that for $r = -|r_0|$. Thus, we are further justified in taking $r \in (0,1)$ as we argued initially in Section III-B. In general, we must calculate Γ from Eq. (143). However, in the next section we shall show that in most cases of interest, we can approximate Γ quite well by a simple expression.

B. Narrowband Approximation

We see in Fig. 13 that for values of r near unity that the area of $W(f)$ becomes concentrated near $f = f_m$. We know that in almost all cases of interest we will have $P/\tau \ll 1$ so that r is near unity. We thus realize that in these cases we can approximate $W(f)$ with delta functions at $f = f_m$ and $f = -f_m$, if $S_F(f)$ is reasonably smooth near $f = f_m$. This smoothness has been observed, so we are justified in taking $W(f)$ as a pair of delta functions. We now need to find the area near $f = f_m$ in $W(f)$ so we can approximate $W(f)$ as

$$W(f) = W_0\delta(f+f_m) + W_0\delta(f-f_m) \tag{147}$$

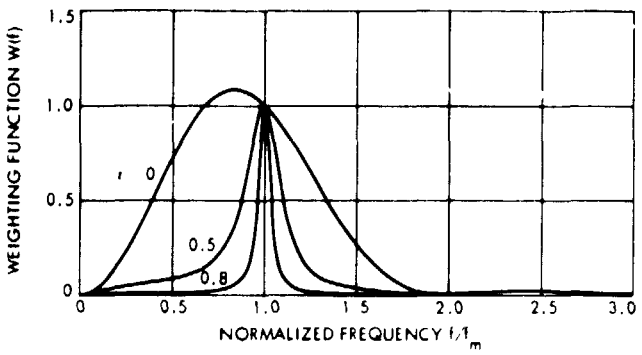

Fig. 13. Weighting function

We note for r near unity that the cosine function in the denominator of Eq. (144) is the principal factor determining the area of $W(f)$. We thus expand the numerator of Eq. (144) around $f = f_m$

$$\sin^2\left(\pi\frac{f+f_m-f_m}{f_m}\right) = \sin^2\left(\pi+\pi\frac{f-f_m}{f_m}\right) \approx \pi^2\left(\frac{f-f_m}{f_m}\right)^2 \tag{148}$$

Also, the first term in the denominator of Eq. (144) can be similarly expanded around $f = f_m$ as

$$\left[1-\left(\frac{f}{f_m}\right)^2\right]^2 \approx 4\left(\frac{f-f_m}{f_m}\right)^2 \tag{149}$$

Using Eqs. (148) and (149) in Eq. (144) we find $W(f)$ near f_m to be given approximately by

$$W(f) \approx \frac{(1-r)^2}{1+r^2-2r\cos(2\pi f/f_m)} \tag{150}$$

Now since W_0 is to be the area of $W(f)$ near $f = f_m$, we can find W_0 by integrating over one period of Eq. (150) as

$$W_0 = \int_{f_m/2}^{(3/2)f_m} W(f)\,df \tag{151}$$

This integration can be carried out and after much manipulation gives

$$W_0 = \frac{1-r}{1+r} f_m \tag{152}$$

From Section III-B, we know $(1-r)/(1+r)$ is well approximated by $P/2\tau$. Using this and the obvious relation $P = 1/f_m$, we have

$$W_0 = 1/2\tau \tag{153}$$

Thus, from Eq. (147)

$$W(f) = \frac{1}{2\tau}\left[\delta(f+f_m) + \delta(f-f_m)\right] \tag{154}$$

and using this in Eq. (143) we have

$$\Gamma = \frac{1}{2\tau}\left[S_F(-f_m) + S_F(+f_m)\right] \tag{155}$$

$S_F(f)$ is an even function, however, so $S_F(-f_m) = S_F(+f_m)$ and we obtain the simple result

$$\Gamma = S_F(f_m)/\tau \tag{156}$$

We refer to the approximations made in this section as a narrowband approximation since by restricting τ to be large the system is responding only to the gain fluctuation noise in a narrow band around f_m. Substitution of Eq. (155) in Eq. (145) gives

$$\sigma = \left[\frac{\frac{T_{OP}}{T_S} + g(R)}{g'(R)}\right]\frac{\left[\frac{1}{B} + S_F(f_m)\right]^{1/2}}{\tau^{1/2}} \tag{157}$$

We now take $g(\beta)$ to be Gaussian as in Eq. (49)

$$g(\beta) = \exp\left[-\mu(\beta/W)^2\right] \tag{158}$$

Substitution in Eq. (157) gives

$$\sigma = \frac{1 + \frac{T_{OP}}{T_S} e^{\mu(R/W)^2}}{2\mu R/W^2}\,\frac{\left[\frac{1}{B} + S_F(f_m)\right]^{1/2}}{\tau^{1/2}} \tag{159}$$

Use of Eq. (50) for μ and writing this in normalized fashion gives

$$\boxed{\frac{\sigma\tau^{1/2}}{W\left[\frac{1}{B} + S_F(f_m)\right]^{1/2}} = (0.180)\frac{1 + \frac{T_{OP}}{T_S} e^{(2.773)(R/W)^2}}{R/W}} \tag{160}$$

This normalized function is the same as that in Eq. (52) except for the presence of $S_F(f_m)$, so Fig. 7 can be used for evaluation. We present this result in Fig. 14. We thus have the rms error in the elevation axis as σ. By symmetry the error in the cross-elevation axis is the same. The simplicity of this result is impressive. We see that when $\tau \gg P$ and $S_F(f)$ is smooth, only $S_F(f_m)$ is needed in order to evaluate σ. It is interesting to note that σ varies inversely with τ, for arbitrarily large values of τ. In addition, we see that gain fluctuations prevent one from achieving arbitrarily small σ by making B very large. We see, in fact, that if $1/B$ is comparable to $S_F(f_m)$ we can decrease σ only by an additional factor of $\sqrt{2}$ even if $B \to \infty$. Since $S_F(f)$ is almost always monotonically decreasing, we can also see mathematically the decrease in σ which can be obtained by increasing f_m. It is necessary, of course, to know $S_F(f)$ before σ can be calculated.

We have modeled the beam shape as Gaussian so the crossover loss was found in Eq. (53) to be

$$g(R) \text{ in dB} = 12.04(R/W)^2 \tag{161}$$

and was plotted in Fig. 8. In Fig. 15, we present σ in Eq. (160) cross-plotted against the crossover loss $g(R)$. In this plot it is easy to see the tradeoff of σ vs $g(R)$.

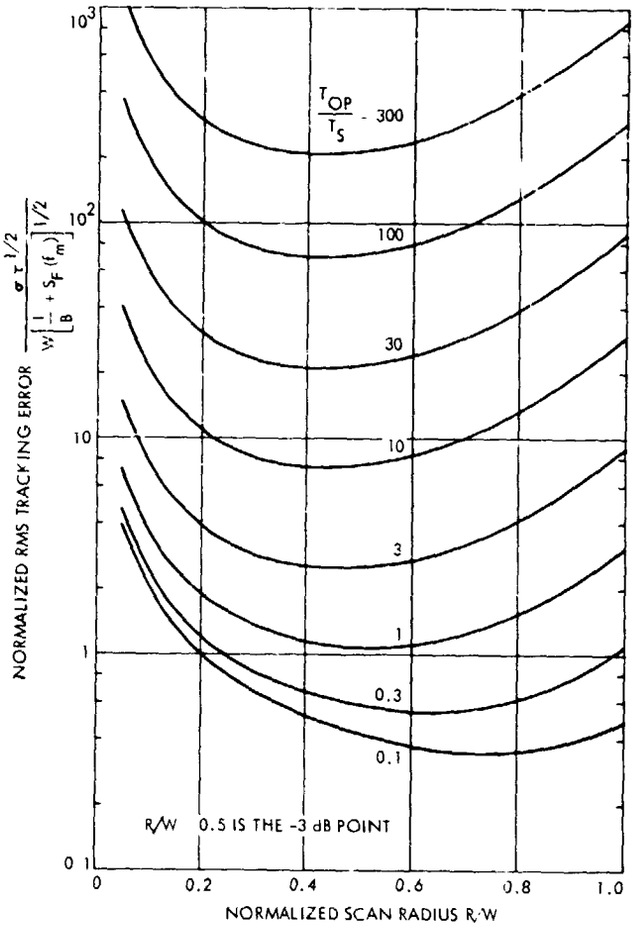

Fig. 14. Radio source angular tracking error

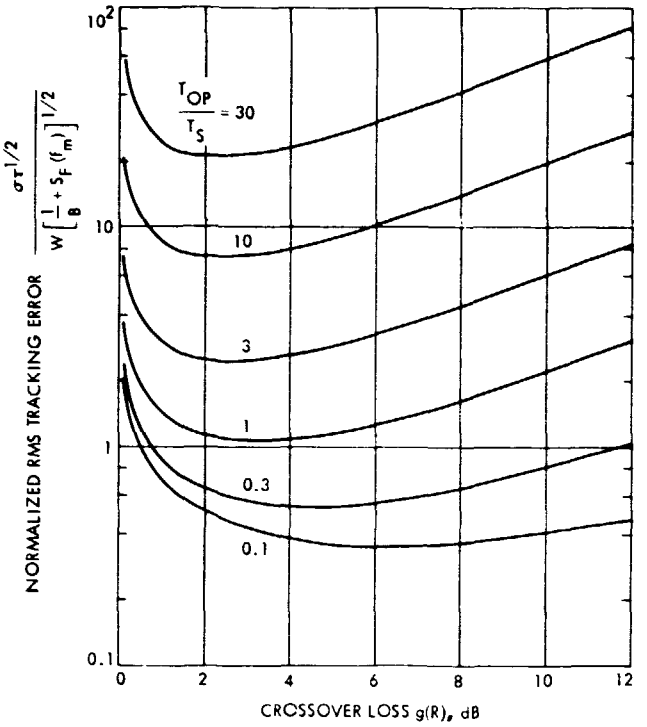

Fig. 15. Radio source angular tracking error vs crossover loss

C. Tracking of Spacecraft

We assume as in Section IV that the receiver is either in MGC or compensation has been made for the effects of AGC upon the error signal. We saw in Eq. (108) that the system voltage gain varies as $[1+F(t)/2]$ so we take the signal strength $x(t)$ in Eq. (73) and multiply by this factor to obtain

$$x'(t)=\left[1+F(t)/2\right]x(t) \tag{162}$$

$$=K\left[1+F(t)/2\right]\sqrt{P_S}\,v(t)$$

$$+\left[1+F(t)/2\right]Kn'(t) \tag{163}$$

We can ignore $F(t)$ in the second term of Eq. (163) since it gives only a very small variation to the effect of $n'(t)$. In the first term of Eq. (163) we can determine an average value of $v(t)$ as far as $F(t)$ is concerned. Looking at Eq. (63) and realizing that usually $\theta,\phi \ll R$, then

$$\text{average}\left[v(t)\right]\approx\exp\left[-\mu'(R/W)^2\right] \tag{164}$$

(If θ and ζ are not $\ll R$, we will usually be able to assume the average is ≈ 1.) Using the above approximations, we have

$$x'(t)=\Lambda F(t)+x(t) \tag{165}$$

where

$$\Lambda=\frac{K\sqrt{P_S}}{2}\exp\left[-\mu'(R/W)^2\right] \tag{166}$$

We now form $\Delta_k^{(c)}$ and $\Delta_k^{(s)}$ as in Eqs. (113) and (114), using the argument after those equations to write the integral limits as $[(k-1)P, kP]$. We obtain for the elevation case

$$\Delta_k^{(c)}=-h\left[K\sqrt{P_S}\,d_k+N_k^{(c)}\right]+m_k^{(c)} \tag{167}$$

where

$$d_k=\int_{(k-1)P}^{kP} v(t)\sin\omega_m t\,dt \tag{168}$$

$$N_k^{(c)}=K\int_{(k-1)P}^{P} n'(t)\sin\omega_m t\,dt \tag{169}$$

$$m_k^{(c)}=-h\Lambda\int_{(k-1)P}^{kP} F(t)\sin\omega_m t\,dt \tag{170}$$

In Section IV, using Eqs. (77)–(90), d_k is evaluated so we can rewrite Eq. (167) as

$$\Delta_k^{(c)}=-h\left[A\phi_k+N_k^{(c)}\right]+m_k^{(c)} \tag{171}$$

where, as in Eq. (92),

$$A=\frac{KP\mu R\sqrt{P_S}}{2W^2}\exp\left[-\mu'(R/W)^2\right] \tag{172}$$

The $N_k^{(c)}$ are independent random variables with variance σ_N^2 given in Eq. (95). Equation (171) is now in exactly the same form as Eq. (115), with $m_k^{(c)}$ in Eq. (170) identical to Eq. (116). The only difference is that A is given by Eq. (172) rather than Eq. (19) and σ_N^2 is given by Eq. (95) rather than Eq. (22). We may thus follow our previous work from Eq. (115) on down to Eq. (140).

We now substitute $h=(1-r)/A$ from Eq. (28), Λ from Eq. (166), and A from Eq. (172) and using Eq. (141) we have

$$\sigma_g^2=\frac{W^4}{4\mu^2 R^2}\Gamma \tag{173}$$

where Γ is as in Eq. (143). From Eq. (127), where σ_ϕ is taken from Eq. (98), we have the rms tracking error given by

$$\sigma=\frac{W^2}{\mu R}\left[\frac{k\,T_{OP}e^{\mu(R/W)^2}}{P_S 2\tau}+\frac{\Gamma}{4}\right]^{1/2} \tag{174}$$

As in the radio source case, the general case involves the evaluation of Eq. (143) for Γ. However, since r will be near 1, we can invoke the narrowband approximation of Section V-B and have, from Eq. (156),

$$\Gamma=S_F(f_m)/\tau \tag{175}$$

Use of this in Eq. (174) gives

$$\sigma=\frac{W^2}{\mu R\sqrt{2\tau}}\left[\frac{kT_{OP}e^{\mu(R/W)^2}}{P_S}+\frac{S_F(f_m)}{2}\right]^{1/2} \tag{176}$$

We now put σ in normalized form and use Eq. (50) for μ to obtain

$$\frac{\sigma}{W}\left[\frac{\tau}{S_F(f_m)}\right]^{1/2}=(0.180)\frac{\left[1+\dfrac{2kT_{OP}}{P_S S_F(f_m)}e^{2.773(R/W)^2}\right]^{1/2}}{R/W} \tag{177}$$

This result is presented in Fig. 16. We also present this result in Fig. 17 cross-plotted against the crossover loss $g(R)$ in Eq. (161).

It is of interest to compare the rms angle tracking errors for the radio source and spacecraft cases when the system signal-to-noise ratio becomes very large and only the gain fluctuations limit performance. In Eq. (160), if we take B and T_S to be infinite, we get the same result as when we take $P_S\to\infty$ in Eq. (177). This is not a coincidence since

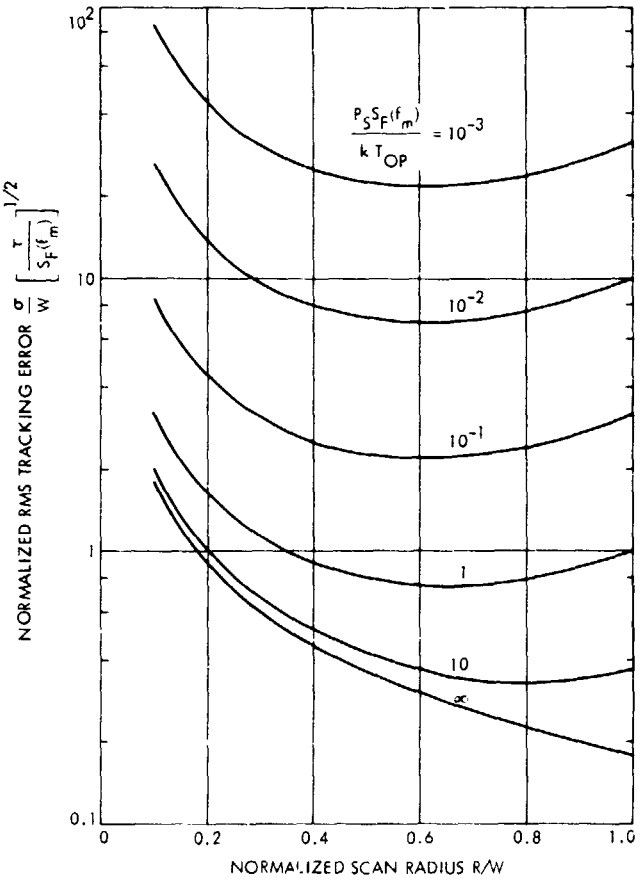

Fig. 16. Spacecraft angular tracking error

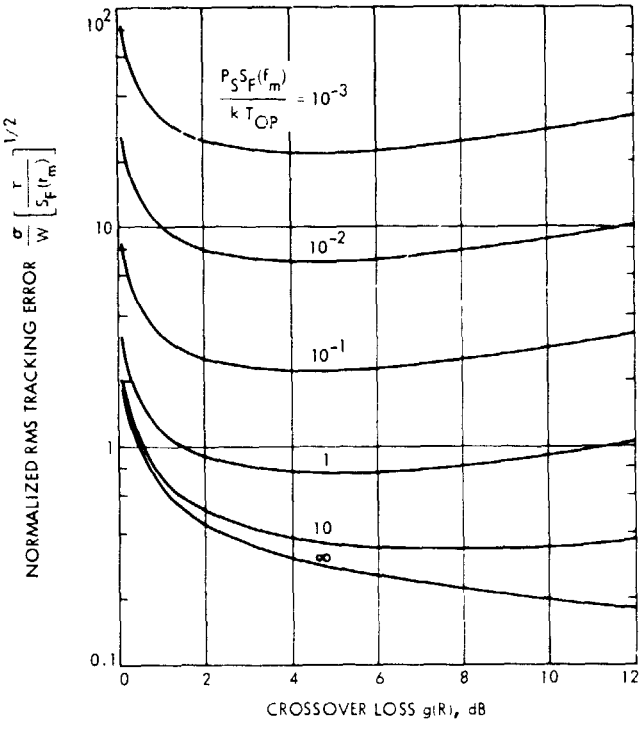

Fig. 17. Spacecraft tracking error vs crossover loss

we *should* get the same result when the only limitation is the system gain fluctuation.

VI. Experimental Implementation at the Goldstone 64-m-diameter Antenna

In the period 1972–1974, an experimental implementation of the conical-scan scheme was made on the NASA/JPL 64-m-diameter antenna Mars Station (DSS-14). The system worked well for tracking of both spacecraft and radio sources. The system has been used extensively in an operational quasi-manual mode for tracking since the initial installation. A fully automatic operational conical-scan program is now being developed for regular use in the Deep Space Network.

A. Conical-Scan Hardware

The conical-scan system is easily broken down into hardware and software blocks. The hardware diagram is shown in Fig. 18. The system permits any of five signals to be used as conical-scan "signal strength" data. The broadband square law detector (Ref. 8) can be used with any of the RF front-ends on the antenna. The four receivers at DSS-14 each have their AGC voltage brought to the Multi-Channel-Analog-Signal-Conditioner (MCASC). The MCASC consists of a separate DC amplifier, lowpass filtering and level shifting for each channel. The purpose is to bring each of the input lines into a range compatible with the analog-to-digital converter (ADC). The ADC has 12 conversion bits including sign, and it samples 10 times per second. So that there is less than 4% decrease in SNR due to the finite sampling rate of the ADC, the time constant of the MCASC must then be 0.1 s and it is set accordingly (Ref. 9). It is also desirable that quantization noise not be a limiting factor. Thus there must be enough gain prior to the ADC, and the ADC must have enough levels so that the voltage into the ADC randomly crosses several levels due to noise alone. A 12-bit ADC was found to be adequate for a wide range of signal types.

B. Conical-Scan Software

The computer used for the Antenna Pointing System (APS) at DSS-14 is a Scientific Data Systems SDS 910. The conical-scan program was packed into approximately 2000 24-bit locations which were available after the primary APS program was placed into core. The conical-scan program is an option which is selectable by an operator by using a breakpoint switch.

A block diagram of the computer calculation is shown in Fig. 19. The program was configured so it could do a conical scan in either hour angle/declination (HA/DEC) or azimuth/elevation (AZ/EL) coordinates. The appropriate secant correction is required in either case so as to get a circular scan as seen as a projection on the celestial sphere. The operation is easy to follow. Consider an AZ/EL scan. The scan frequency in radians/second is $\omega_m = 2\pi/P$. The AZ scan $R\sin\omega_m t$ is corrected by the secant of EL and is fed to the antenna pointing function along with the EL scan $R\cos\omega_m t$ and the computer predicts for boresight. This then results in a conical scan. The square-law detector or an AGC voltage feeds the ADC which is then multiplied by in- and out-of-phase scan sinusoids and is integrated (summed) for one scan. A gain h is applied and a teletype printout occurs. If the loop is closed, an angular position correction to boresight is made and tracking commences. When the system is in closed loop operation, the teletype prints the accumulated total of corrections. The phase shift θ is necessary due to phase

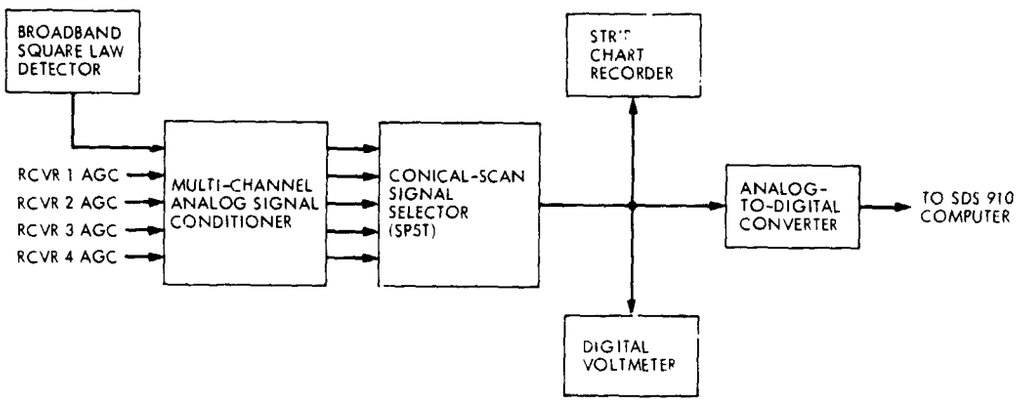

Fig. 18. Conical-scan hardware

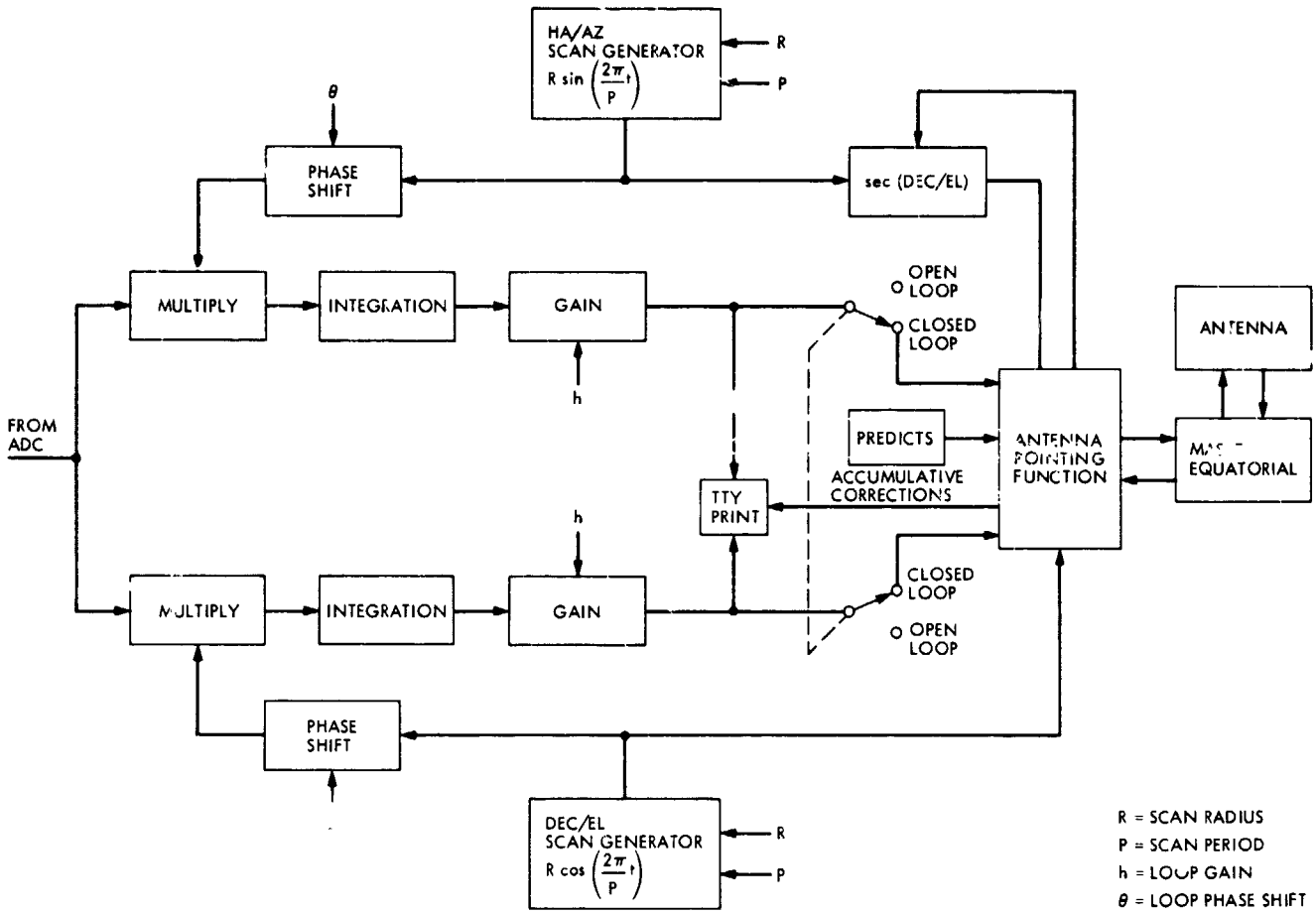

Fig. 19. Conical-scan software

lag in the physical antenna and the AGC loop or detector filter. The value of θ is determined experimentally so that the two channels decouple and work independently.

It was found that the primary source of phase lag is actually the antenna itself. A circular scan requires sinusoidal acceleration in each axis, and the antenna servo cannot achieve zero steady state position error. For a 28-s scan, θ needs to be about -30 deg and for a 58-s scan has to be about -15 deg in order to decouple the two axes. The value of the scan radius R is chosen so that the crossover loss is acceptable for the task at hand. For the experimental program, each scan had a 2-s halt to allow all calculations to be completed. It was not convenient to remove this halt, but little error was so introduced because

Table 2. Primary classes of use

Purpose	Scan radius	Crossover loss, dB	Response
Maximize gain	Small	< 0.1	Slow
Look at dynamics (e.g., repeatable errors and wind effects)	Large	$2-3$	Fast

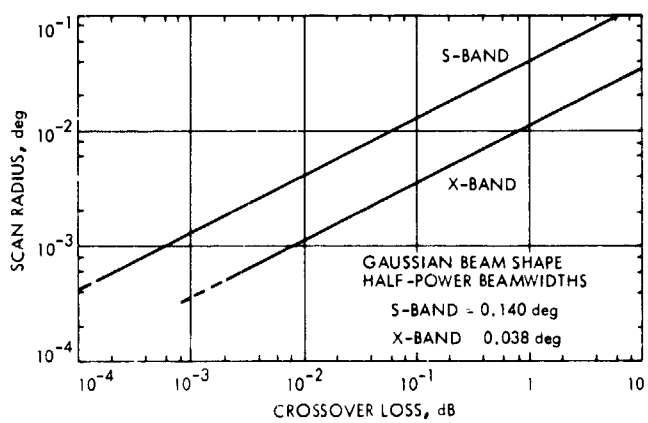

Fig. 20. Crossover loss vs scan radius

Table 3. Tracking error tests

Test	Source	Frequency	Scan radius, deg	Crossover loss, dB	Scan period, s	No. of scans	rms spread, deg	Comments
A	3C123	S-band	0.010	0.06	28	8	0.00015	Limited data
B	3C123	S-band	0.010	0.06	28	30	0.00035	
C	3C123	S-band	0.020	0.25	18	10	0.00015	Antenna jerky, probably too short a scan period. Limited data.
D	3C123	X-band	0.002	0.033	28	5	0.0002	Little data; however, manual hunting could only pick up 0.02 dB.
E	Pioneer 9	S-band	0.040	1.0	28	6	0.00032	Limited data.
F	Pioneer 9	S-band	0.040	1.0	28	8	0.00035	Limited data.
G	Pioneer 9	S-band	0.013	0.1	28	18	0.0004	
H	Pioneer 9	S-band	0.013	0.1	28	17	0.00035	

the antenna tended to coast through the halt. The value of G is "large" for fast response and "small" for long averaging times. Two primary classes of use exist as shown in Table 2. For ease of relating scan radius to crossover loss, Fig. 20 is convenient for S-band (≈2300 MHz) and X-band (≈8400 MHz) frequencies.

C. Experimental Results

Two types of data will now be shown—pull-in transients and rms error statistics. In Fig. 21 is shown the pull-in transient on the radio source 3C123 with the S-band beam when the initial error is approximately −0.020 deg in declination. This source gives about 22 kelvins on the 64-m-diameter antenna at S-band. In Fig. 22 is shown a pull-in transient on the Pioneer 9 spacecraft when initial errors were sizable in both coordinates and the initial condition represented a gain loss of 4 dB.

In Table 3 are shown the results of a series of tests performed on October 25, 1973, using HA/DEC scanning. The crossover loss is taken from Fig. 20. The number of scans shown is the number which was observed after any initial transient subsided. The rms spread is taken as one-sixth of the peak-to-peak variation observed. In most cases HA and DEC spreads were comparable. If they were not, they were averaged. These data are quite crude and obviously are not compensated for any systematic errors. However, the rms spreads are remarkably consistent and may indicate a lower limit to the attainable accuracy. In Table 3, only tests B, G and H have a large enough number of scans so the rms spread is of value. To get more information on the validity of this rms spread, refer to Table 4. Tests A, B and C in Table 3 are all on 3C123. For all times during A, B and C when the system was tracking in steady state operation, the overall peak-to-peak variation of absolute tracking error vs predicts was tabulated. One-sixth of this range is estimated as the rms error. The same procedure was applied to the block of tests E, F, G and H. Considering that the peak-to-peak range observed certainly includes systematic errors of the antenna due to the long duration, the rms variation in Table 4 probably is a very conservative upper bound on the random component of tracking error. It is of interest to note that the resolution of the encoders on the master equatorial is about 0.0003 deg and their accuracy is on the order of 0.001 to 0.002 deg. These data indicate a probable rms tracking accuracy for moderate strength signals like 3C123 and Pioneer 9 of better than a thousandth of a degree. This will be discussed further in Section VI-E.

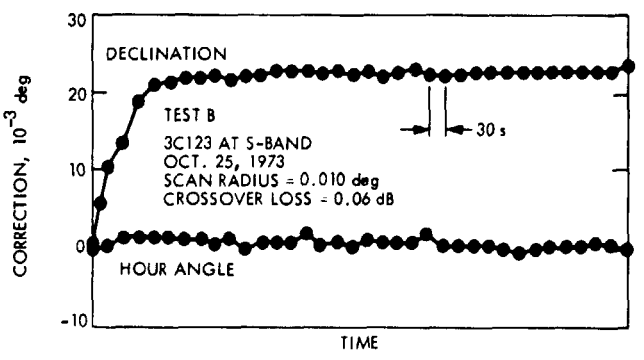

Fig. 21. Conical-scan pull-in on radio source 3C123 at S-band

Table 4. Overall rms variation

Tests	Time span	Observed rms Variation, deg		Comments
		Hour angle	Declination	
A, B, C	1 h, 13 min	0.00096	0.00052	Begun 1 h after meridian transit.
E, F, G, H	1 h, 59 min	0.00073	0.00056	Straddled meridian transit.

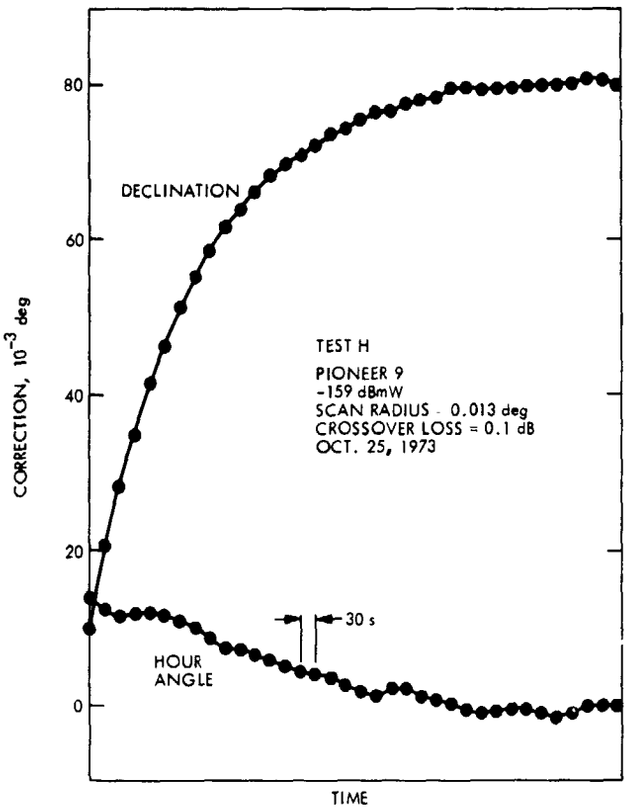

Fig. 22. Conical-scan pull-in on Pioneer 9 spacecraft

D. Operational Manual Mode

As the Mariner Venus/Mercury 1973 (Mariner 10) encounters approached, it was decided to make operational for X-band tracking a portion of the experimental conical-scan system. The antenna was put into a 58-s scan with a radius of 0.004 deg having a crossover loss ≈0.14 dB. The operator could then average the open loop printouts to decide when a correction should be manually entered. Alternatively, he could watch the strip chart recorder shown in Fig. 18. As boresight would drift off the spacecraft, a sinusoidal pattern would appear on the strip chart and the operator could search with HA and DEC corrections to null it out. This mode of operation has continued through to 1976.

E. Tracking Data From Mariner Venus/Mercury 1973

During the spring 1974 tracking period of Mariner 10 considerable tracking time was accumulated in the operational manual mode of conical-scan tracking, as described above. Each time the operator zeroed the errors, an entry was made in a log. In order to get an idea of the potential of conical scan (when eventually made fully automatic)

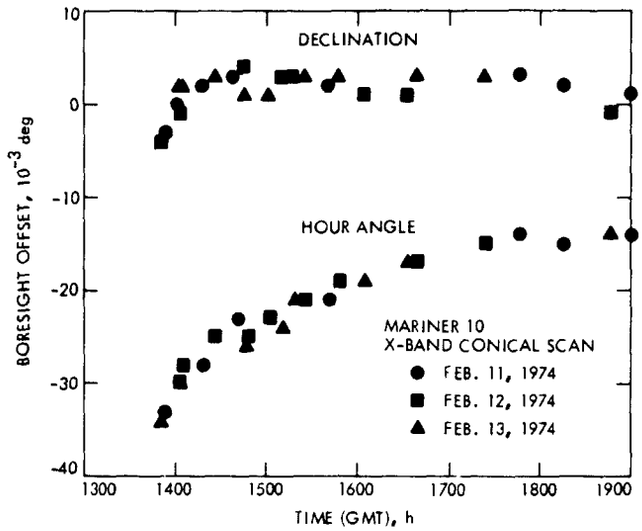

Fig. 23. Mariner 10 offsets, February 11–13, 1974

these log sheets have been reduced to give corrections in AZ/EL as well as HA/DEC coordinates and various plots were made to try to uncover correlations.

First, considering repeatability, in Fig. 23 is shown the set of raw manual corrections vs time (GMT) for 3 consecutive days. The agreement is within about 0.003 deg for the worst case. In Figs. 24 and 25 are shown further 3-day plots. Consecutive-day data would be expected to show repeatable daily variations, as they do. The worst case discrepancy is 0.005 deg for a 1 sigma statistic of less than 0.001 deg. This is impressive. The consistency indicates that a fully automatic conical-scan system will almost certainly achieve the rms error of less than 0.001 seen in Section VI-C.

In Fig. 26, elevation offsets vs azimuth are shown for March 23–25, 1974. Consistency is again shown, as well as a distinct hint that the ionospheric refraction correction is

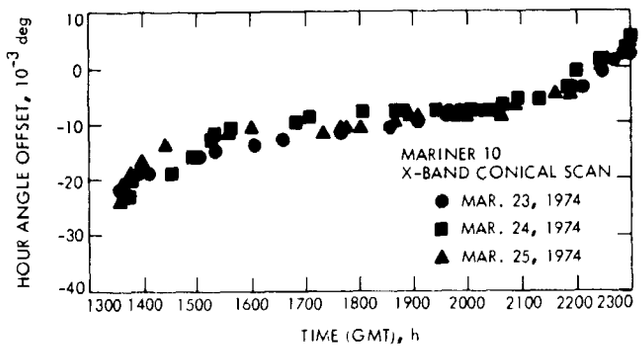

Fig. 24. Mariner 10 hour angle offsets, March 23–25, 1974

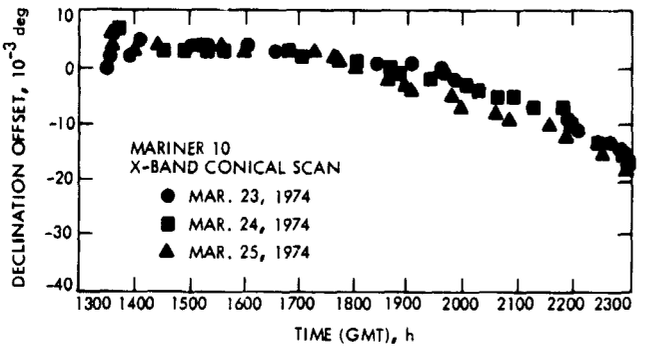

Fig. 25. Mariner 10 declination offsets, March 23–25, 1974

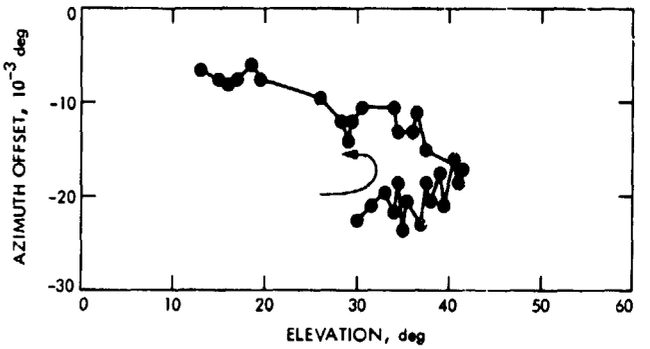

Fig. 27. Mariner 10 azimuth offsets vs elevation, February 4, 1974

in error for low elevation angles, i.e., when AZ is less than 140 deg and greater than 240 deg. (A new refraction correction program is being prepared at this time.)

Many plots were made of ΔAZ vs AZ, ΔAZ vs EL, ΔEL vs AZ and ΔEL vs AZ. The curves obtained were reasonably consistent for consecutive days and/or weeks. However, over the roughly four months' period for which much data was taken, only the ΔAZ vs EL plots gave a consistent pattern over the whole time. There are 24 days in this period for which a "complete" track was made—e.g., low elevation to high elevation to low elevation. Every plot of ΔAZ vs EL showed a characteristic sideways "U". Figs. 27–31 are typical of this group. The arrow indicates time through the track. No reasonable explanation is offered for this characteristic shape; it may be a twisting hysteresis arising in the rising/falling antenna structure, but the continuous conical scanning would seem to break up such a hysteresis effect. The sides of the U became farther apart as summer approached. This is probably related to the secant correction for higher elevation angles. The U shape may be refraction-connected. In any event it shows the extent to which conical scanning can correct for anomalies, whatever their source.

The data from the logs were subjected to a statistical correlation procedure to see if wind effects could correlate with any observed offsets. The results were generally inconclusive, although on windy days the data seemed to scatter more. With a fully automatic conical-scan system, the response time can be faster so wind effects can be more reliably observed. The problem of correlating systematic errors with this antenna is made difficult by the

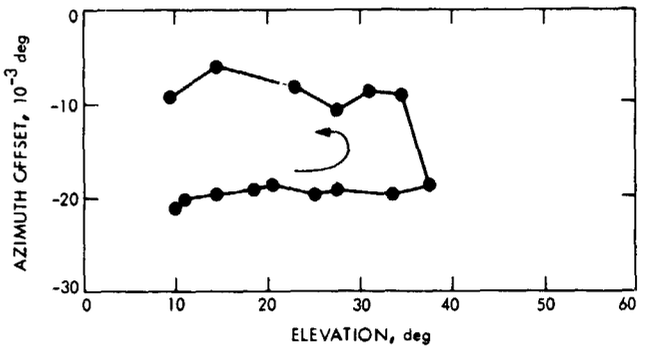

Fig. 28. Mariner 10 azimuth offsets vs elevation, February 13, 1974

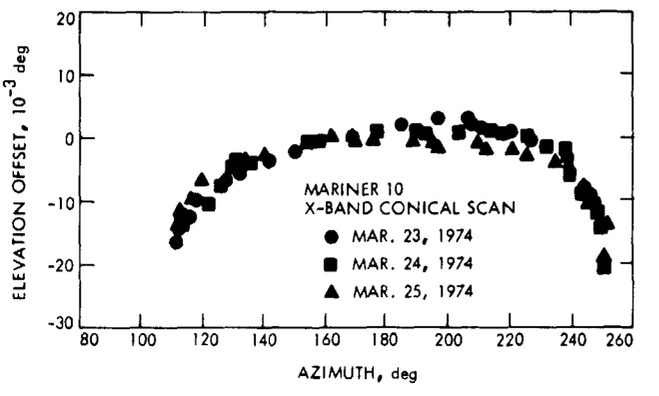

Fig. 26. Mariner 10 elevation offsets vs azimuth, March 23—25, 1974

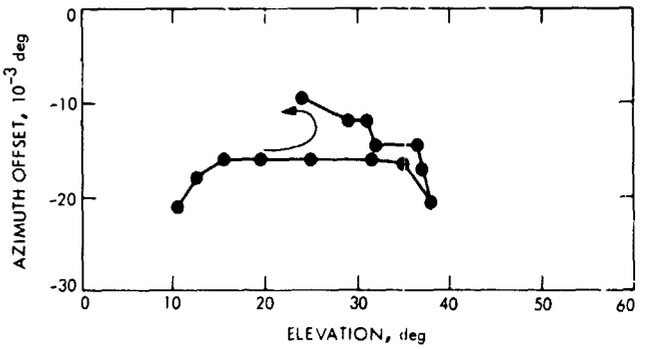

Fig. 29. Mariner 10 azimuth offsets vs elevation, March 8, 1974

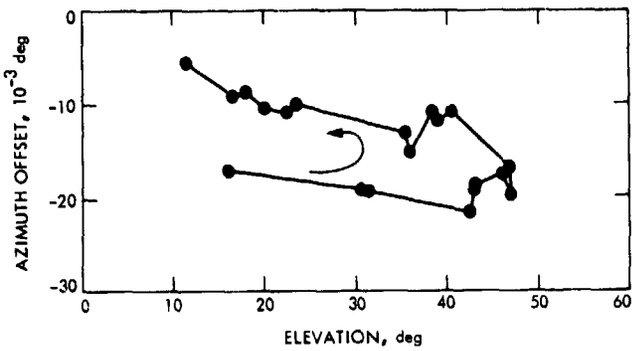

Fig. 30. Mariner 10 azimuth offsets vs elevation, April 1, 1974

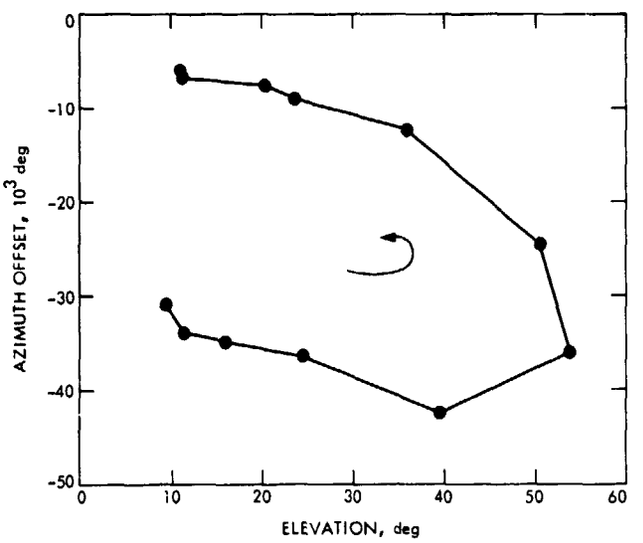

Fig. 31. Mariner 10 azimuth offsets vs elevation, April 11, 1974

fact that the antenna itself is an AZ/EL mount, while the Master Equatorial is of HA/DEC type.

F. Comparison of Experimental and Theoretical Accuracy

We are able to make comparisons of the experimental and theoretical accuracies for Tests B, G and H of Table 3 and for the Mariner 10 data. The parameters of these tests are given in Table 5. The value of τ for B, G and H was taken from observation during pull-in, while for Mariner 10 it represents a reasonable guess as to the operator's visual averaging time. In Table 6 the theoretical and experimental rms errors are compared. The theoretical values ignore gain variations by letting $S_F(f_m)$ be zero in Eqs. (160) and (176). The rms error for Mariner 10 is deduced in Section VI-E. The overall rms column is an average of the HA and DEC values in Table 4.

Table 5. Test parameters

Parameter	Test B	Test G, H	Mariner 10
R	0.010 deg	0.013 deg	0.004 deg
W	0.140 deg	0.140 deg	0.038 deg
τ	75 s	200 s	300 s
T_{OP}	20 K	20 K	20 K
T_s	22 K	—	—
B	10 MHz	—	—
P_s	—	−159 dBmW	−144 dBmW

Table 6. Experiment vs theory

Test	Theoretical rms, 10^{-3} deg	Observed rms, 10^{-3} deg	Overall rms, 10^{-3} deg
B	7.8×10^{-6}	0.35	0.74
G, H	1.3	0.35, 0.4	0.65
Mariner 10	0.045	<1	<1

Some interesting conclusions may be drawn from these data. First, the observed rms errors are all about the same for three vastly differing conditions with greatly different theoretical accuracies. This indicates that encoder errors and/or gain fluctuations are the primary limitations on tracking accuracy. Second, some of the error observed might be systematic in nature and the rms error observed may not be entirely random. Third, the theoretical value of rms error for radio source tracking will be very small due primarily to the $1/B$ term in Eq. (160). This small value will not be achieved with the present system.

VII. Conclusions

A thorough analysis of a conical-scan system suitable for large antennas has been made. Details of an experimental implementation were given and tracking data were presented. Tracking accuracies of 0.001 deg rms seem to be readily obtainable.

References

1. Gosline, R. M., "CONSCAN Implementation at DSS 13, " *The Deep Space Network Progress Report*, Technical Report 32-1526, Vol. XIV, pp. 87–90, Jet Propulsion Laboratory, Pasadena, Calif., April 15, 1973.
2. Skolnik, M. I., *Introduction to Radar Systems*, pp. 166–175, McGraw-Hill, New York, 1962.
3. Levy, G., Jet Propulsion Laboratory, Pasadena, Calif., private communication.
4. Kraus, J. D., *Radio Astronomy*, pp. 241–244, McGraw-Hill, New York, 1966.
5. Viterbi, A. J., *Principles of Coherent Communication*, McGraw-Hill, New York, 1966.
6. Abramowitz, M., and Stegun, I. A., *Handbook of Mathematical Functions*, p. 376, 9.6.34, Dover, New York, 1964.
7. Ohlson, J. E., "Exact Dynamics of Automatic Gain Control," *IEEE Transactions on Communications*, Vol. COM-22, No. 1, pp. 72–75, January 1974.
8. Reid, M. S., Gardner, R. A., and Stelzried, C. T., *A New Broadband Square Law Detector*, Technical Report 32-1599, Jet Propulsion Laboratory, Pasadena, Calif., Sept. 1, 1975.
9. Ohlson, J. E., "Efficiency of Radiometers Using Digital Integration," *Radio Science*, Vol. 6, No. 3, pp. 341–345, March 1971.

Appendix

Calculation of the Statistics of $N_k^{(e)}$ and $N_k^{(c)}$

The means of $N_k^{(e)}$ and $N_k^{(c)}$ must be zero because $n(t)$ was assumed to be white. From Eq. (20),

$$\sigma_N^2 = \mathrm{Var}\left[N_k^{(e)}\right] = E\left[\int_0^P \int_0^P n(t_1)n(t_2)\sin\omega_m t_1 \sin\omega_m t_2\, dt_1\, dt_2\right]$$

$$= \int_0^P \int_0^P R_n(t_1 - t_2)\sin\omega_m t_1 \sin\omega_m t_2\, dt_1\, dt_2 \tag{A-1}$$

where $E[\cdot]$ denotes expectation and $R_n(\tau)$ is the autocorrelation function of $n(t)$. From Eq. (13),

$$R_n(t_1 - t_2) = C^2\left[T_{OP} + T_S g(R)\right]^2 B\delta(t_1 - t_2) \tag{A-2}$$

since a Fourier transform relation exists between $S_n(f)$ and $R_n(\tau)$. Putting Eq. (A-2) in Eq. (A-1) and integrating, we have

$$\sigma_N^2 = C^2\left[T_{OP} + T_S g(R)\right]^2 BP/2 \tag{A-3}$$

Similar manipulation shows that $\mathrm{Var}[N_k^{(c)}]$ is also σ_N^2.